Geophys. J. R. astr. Soc. (1975) **43**, 387–424

An Analysis of Near-Bottom Magnetic Anomalies: Sea-Floor Spreading and the Magnetized Layer*

K. D. Klitgord†, S. P. Huestis, J. D. Mudie, and R. L. Parker

(Received 1975 March 6)

Summary

Near-bottom magnetic data over six oceanic ridge segments in the East Pacific are inverted, giving magnetization solutions with alternate positive and negative bands which correspond to geomagnetic field reversals. We estimate the average half-width of the crustal formation zone to be 2–3 km, based on the transition widths between these bands. The solutions show a narrow region of high magnetization centred directly over the centre of spreading, superimposed on a more gradual decrease of magnetization amplitudes with age. Both features are attributed to weathering of highly magnetized pillow lavas. We demonstrate that the short wavelength (<3 km) anomalies are largely due to topography. Distances to reversal boundaries give distance *vs* age curves for each ridge which show that spreading changes occur as sudden accelerations typically separated by several million years of very constant motion. These rate changes are probably accompanied by shifts in the locations of poles of relative motion, which are necessary in a system of more than two interacting plates. Palaeomagnetic data and reversal boundary locations from near-bottom and surface data are combined to give spreading half-rates and a refined time scale for the past 6 My. Widespread spreading rate variations occurred at 2–3 MyBP and about 5 MyBP, possibly as a response to large scale changes in the plate pattern.

1. Introduction

The magnetization of the oceanic crust generated at mid-ocean ridges contains a record of the reversal history of the geomagnetic field, and reflects the manner in which the basaltic upper layer was formed and the alterations of the layer's magnetic properties that have occurred after this formation. The correlation of marine magnetic data from different oceanic ridges allows the separation of world-wide changes in the magnetic field from more local effects, such as spreading-rate variations and magnetization amplitude variations, resulting from the generation and alteration of the magnetized layer. There has been a considerable amount of work on the development of a geomagnetic time scale and the search for short events, but there has been much less consideration of the other information in the marine magnetic anomalies. This has resulted partly from the limited resolution of surface ship magnetic data and partly from the lack of appropriate methods for efficiently analysing the magnetic data.

*Contribution of the Scripps Institution of Oceanography, new series.

†Present address: Department of Geodesy & Geophysics, Madingley Road, University of Cambridge, Cambridge CB3 0EZ.

The development of rapid analysis methods (e.g. Parker 1973) and the use of near-bottom magnetic data (Spiess & Mudie 1970) eliminate many of those difficulties. In this paper we analyse a large volume of such near-bottom observations; we examine the variations with age of the amplitudes of magnetization of the basaltic upper layer, developing detailed spreading rate histories on different ridges, and estimating magnetizations from anomalies produced by lineated bathymetric features. The magnetizations we calculate show not only the decrease in amplitude with age, reported from dredge samples (Marshall & Cox 1972), but they also confirm the existence of a narrow zone of high magnetization within the central anomaly, a phenomenon that previously had been noted only in a suite of dredge samples from the Mid-Atlantic Ridge (Irving, Robertson & Aumento 1970). Spreading rate variations and asymmetric spreading are investigated with near-bottom and sea-surface magnetic data using a technique that requires a knowledge of the absolute ages of only two reversals. The spreading rates and the near-bottom magnetic data are combined to re-examine the geomagnetic time scale from 0 to 6 MyBP.

2. Near-bottom data

Near-bottom geophysical profiles taken over six different segments of the oceanic ridge system of the Pacific (Fig. 1) with the deep tow instrument package (Spiess &

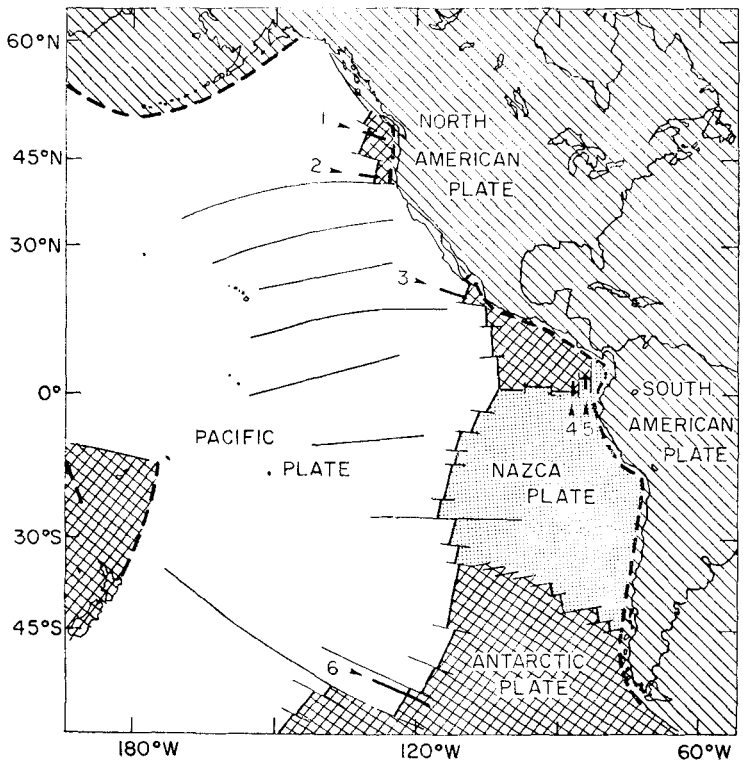

FIG. 1. The plates and mid-ocean ridge system of the Pacific Ocean and the locations of near-bottom geophysical profiles; ———, ridge; ———, transform fault-fracture zone; – – – –, trench; ———<, near- bottom profile: 1—Juan de Fuca Ridge, 47° N; 2—Gorda Rise, 41.5° N; 3—East Pacific Rise, 21° N; 4— Galapagos Spreading Centre, 86° W; 5—Costa Rica Rift, 83° W; 6—Pacific–Antarctic Ridge, 51° S

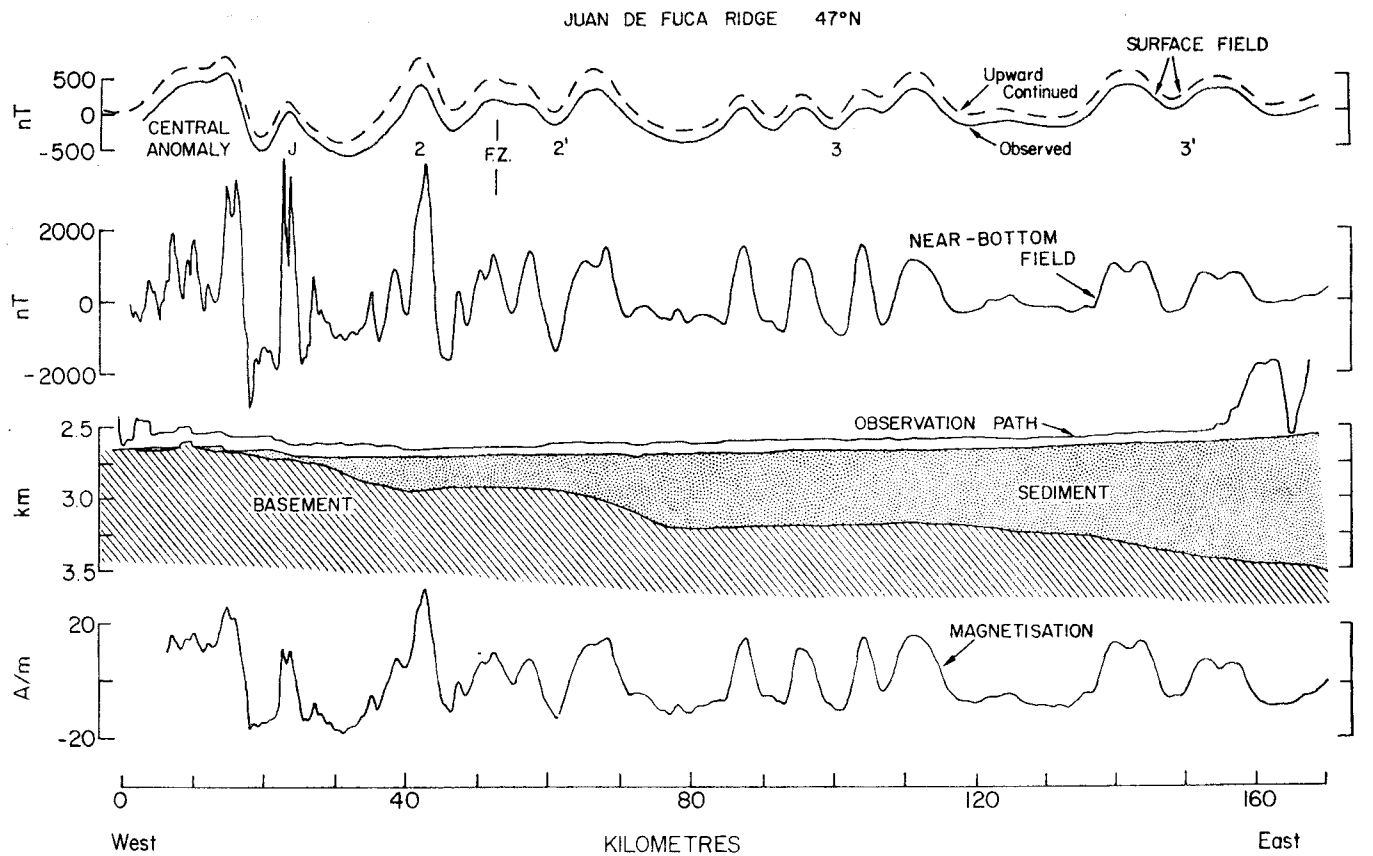

FIG. 2. The near-bottom geophysical profiles over the Juan de Fuca Ridge projected along 120°. At the top is the observed magnetic profile (solid line) with the IGRF removed (IAGA, 1969) and the near-bottom field continued up to the sea surface (dashed line) assuming that it is due to two-dimensional sources and using the method of Parker & Klitgord (1972). The calculated surface field has been displaced from the observed field for the purpose of comparison. In the centre is the observed near-bottom field, with the IGRF removed, taken on the observation path below it. At the bottom is the magnetization distribution calculated with a 0·5 km thick layer by the method of Parker & Huestis (1974).

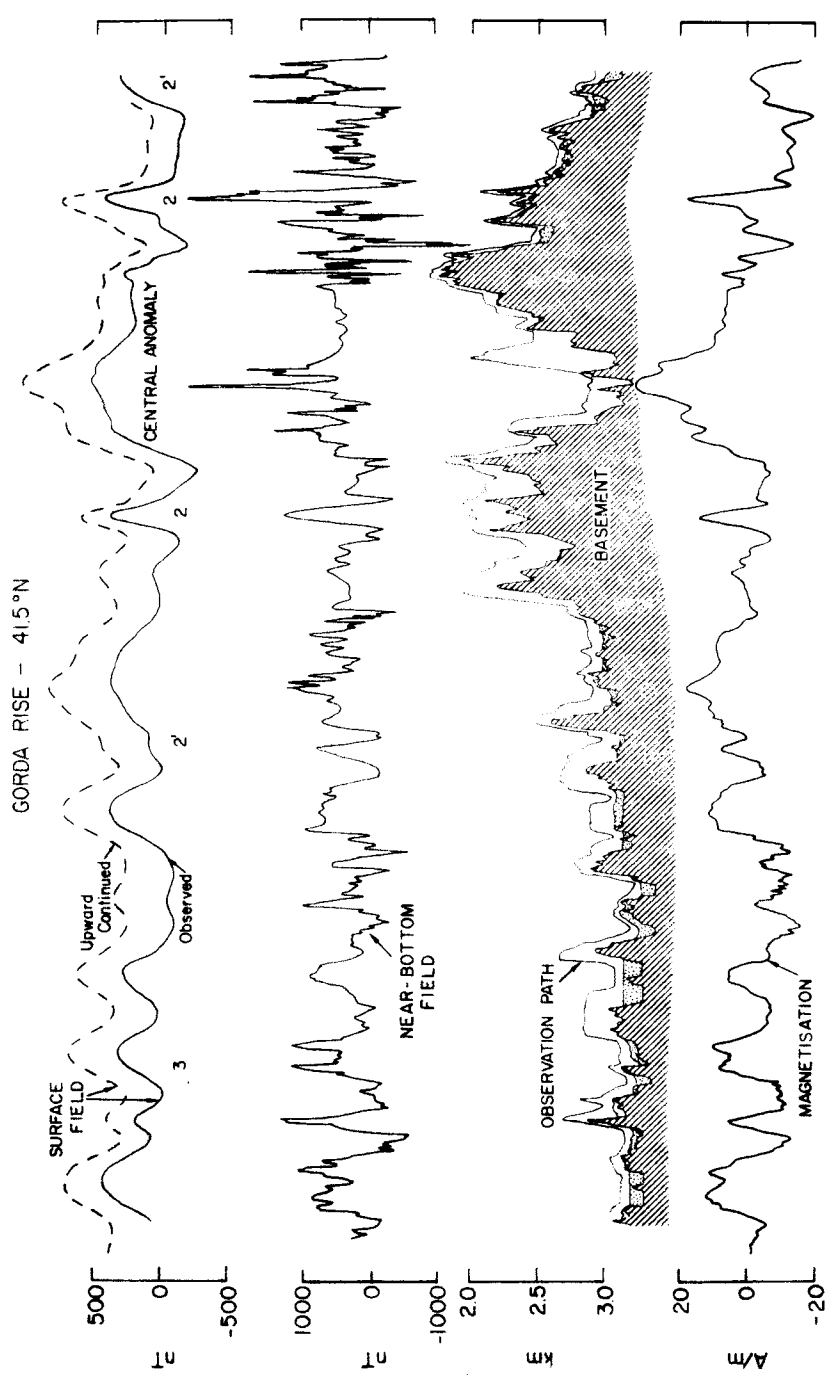

Fig. 3. The near-bottom geophysical profile over the Gorda Rise projected along 100°. See caption of Fig. 2 for details.

Tyce 1973) are the basis for the analyses of marine magnetic data. The magnetic field was measured at intervals of approximately 50 m but, because of the large number of points, the data set was reduced to a sampling interval of 100 m. The sonar systems of the deep tow accurately located the instrument with respect to the ocean floor and, if the sediments were less than 100 m thick, the acoustic basement. Side-looking sonar coverage was used on these long profiles to provide an estimate of the extent or continuity of bathymetric features crossed with the deep tow.

Survey sites

Juan de Fuca Ridge—47° *N.* The Juan de Fuca Ridge (JFR) separates the Pacific plate from one of the remaining parts of the Farallon plate (Atwater 1970). The small Juan de Fuca plate, which forms the eastern flank, is being subducted under the North American plate and numerous small fractures are now disturbing what used to be a more lineated pattern of magnetic anomalies (Peter & Lattimore 1969). The ridge strikes 030° and has a spreading half-rate of about 30 mm/yr. A thick layer of terrigeneous sediments covers the eastern flank (Shor *et al.* 1968) and only the crest of the ridge remains uncovered.

A single deep tow profile (Fig. 2) with satellite navigation was obtained over the sediment-covered eastern flank at 47° N (Spiess & Sanders 1971). Since it was not possible to use the seismic-reflection system while towing, the reflection record at 46·5° N from the *O.S.S. Surveyor* 1971 SEAMAP survey (IDOE 1971) has been used to provide the depth-to-basement control. One of the numerous fractures of the plate was crossed at 47·1° N, 128·3° W (~55 km, Fig. 2), resulting in the younger portion of anomaly 2′ being absent from the profile.

Gorda Rise—41·5°*N.* Just south of the Juan de Fuca Ridge, the Gorda Rise (GR) also is being fractured and rotated as it is subducted under the North American plate and the Mendocino fracture zone (Silver 1969). The strike of the ridge has rotated slowly from 005° to 010° and at about 2 MyBP its spreading half-rate slowed from 37 mm/yr to 12 mm/yr (Atwater & Mudie 1973). Only partly affected by the collision to the east and shielded from the deluge of continental sediments, the western flank has a clear pattern of lineated magnetic anomalies (Raff & Mason 1961) and only a thin sediment cover.

As part of a near-bottom study of the Gorda Rise (Atwater & Mudie 1973), a traverse was made of crust generated from 0 to 5 MyBP (Fig. 3) on the western flank. The navigation, which was by Loran A readings, had errors of up to 3 km in the east–west direction. There is a sharp transition at a distance of 35 km from the centre (Fig. 3) from a fast-spreading ridge with low bathymetric relief to a slow-spreading ridge with large, faulted blocks and a median valley (Atwater & Mudie 1968).

East Pacific Rise—21° *N.* A clear pattern of lineated magnetic anomalies show that the East Pacific Rise (EPR) north of 20° N has been spreading fairly uniformly for the last 6 My at an average half-rate of 30 mm/yr (Larson, Menard & Smith 1968). The ridge, which strikes 010°, has low-amplitude magnetic anomalies because of its orientation and low magnetic latitude. It also has a very low bathymetric relief characterized by small abyssal hills (Menard & Mammerickx 1967).

The western flank was traversed with the deep tow during expedition Oconostotow in 1969 and a near-bottom record was obtained of the magnetic field from 1 to 6 MyBP (Fig. 4). Because only a few star fixes and loran readings were taken during the towing operation, positions are good to only a few kilometres. The sea-floor spreading magnetic anomalies are disturbed at the edge of a large seamount crossed at about 85 km from the centre (Fig. 4).

Galapagos Spreading Centre—86° *W.* The portion of the Galapagos Spreading Centre (GSC) between 85° W and 90° W has been producing high-amplitude lineated magnetic anomalies for the last 3 My (Sclater & Klitgord 1973). The magnetic

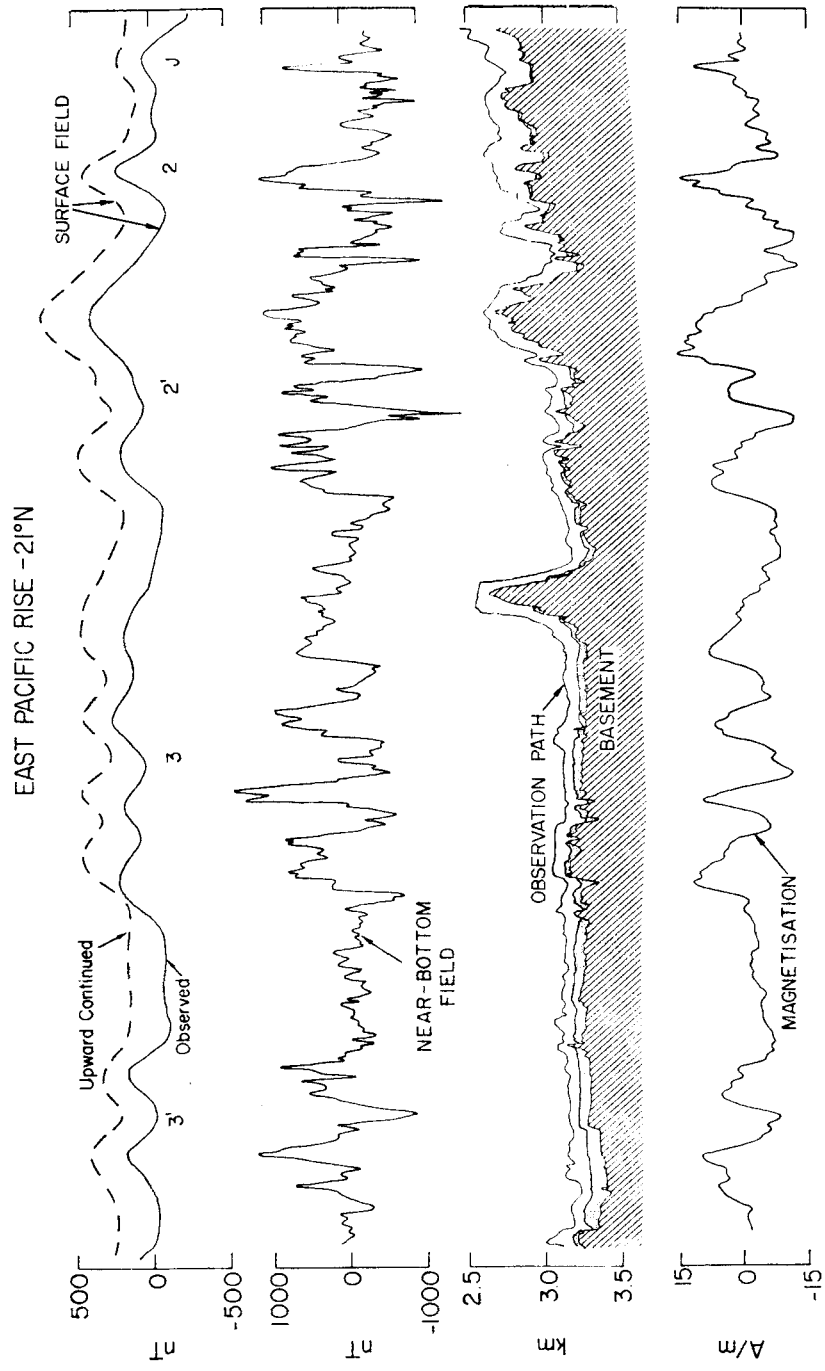

FIG. 4. The near-bottom geophysical profile over the East Pacific Rise projected along 100°. See caption of Fig. 2. for details.

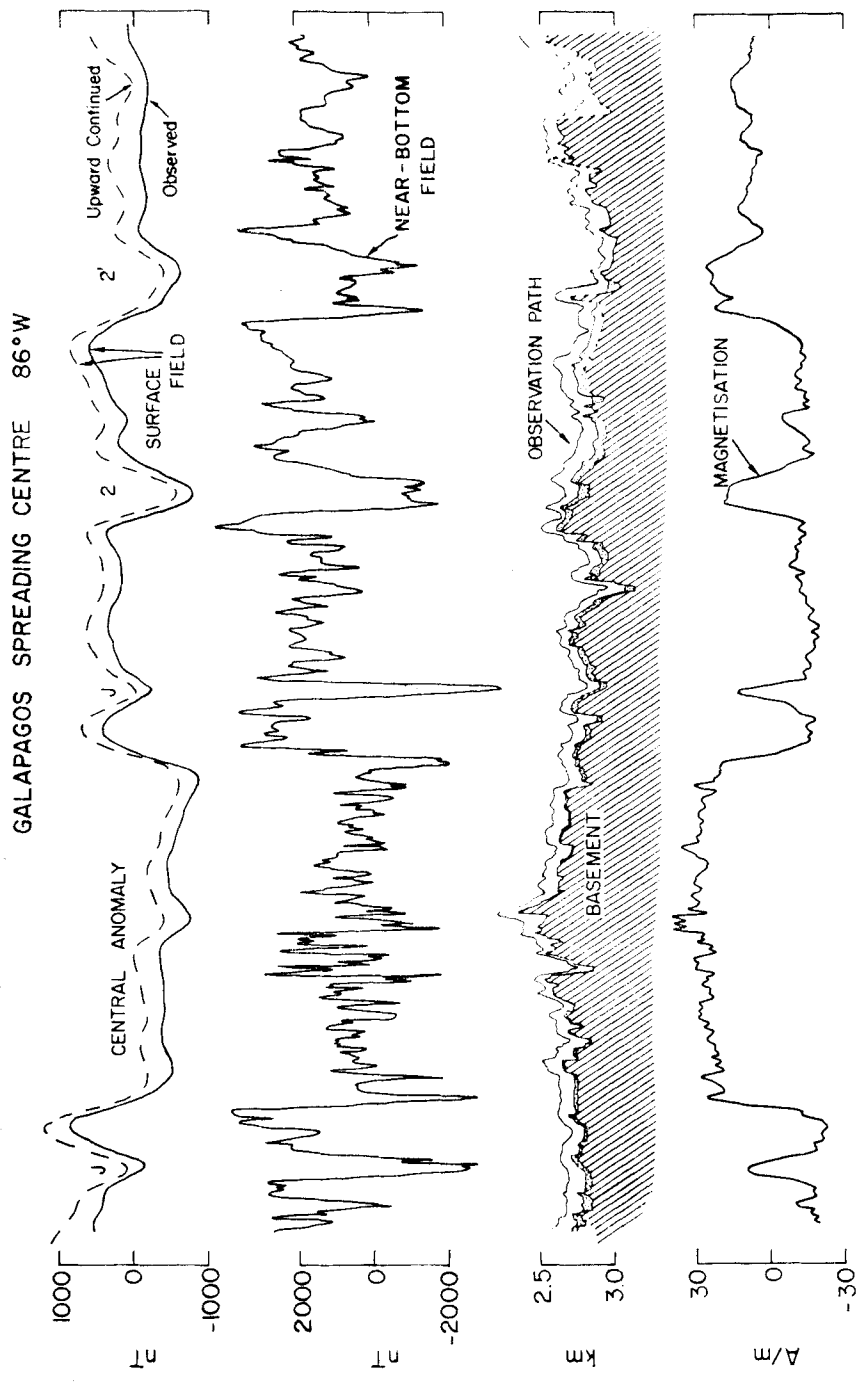

FIG. 5. The near-bottom geophysical profile over the Galapagos Spreading Centre at 86° W projected along 005°. See caption of Fig. 2 for details.

anomalies are exceptionally large in this region perhaps because of the anomalously high titanomagnetite content of the basalts (Anderson *et al.* 1975). The ridge strikes 095° and, because of its fast-spreading half-rate of 35 mm/yr, it has very low relief. Block faulting dominates the relief which becomes more subdued as the sediment cover thickens away fron the spreading centre (Klitgord & Mudie 1974).

A detailed near-bottom survey was conducted over the ridge crest and a long, geophysical profile was obtained from the Jaramillo event on the southern flank to the end of the sea-floor-spreading anomalies at 95 km to the north of the centre of spreading (Fig. 5). Transponder navigation was used from −40 to 10 km (Fig. 5) and and the rest of the profile on the northern flank had satellite navigation.

Costa Rica Rift—83° W. The extension of the Galapagos Spreading Centre to the east, the Costa Rica Rift (CRR), has been an active spreading centre for over 9 My (Grim 1970). It is bounded on the east by the Panama fracture zone at 82·5° W and on the west by the Ecuador fracture zone at 84·5° W. The southern flank appears to terminate at the aseismic Carnegie Ridge while the northern flank is being actively subducted at the Middle America trench (Molnar & Sykes 1969). The total accretion rate has remained at about 72 mm/yr but the half rates on the two flanks have not been equal. There is very low bathymetric relief on the flanks, typical of fast-spreading ridges, while within the centre anomaly a rugged relief is developing.

The satellite-navigated deep-tow profile on the southern flank of this ridge (Fig. 6) shows the low bathymetric relief on the flank contrasting with the two large peaks close to the centre. The rather variable magnetization distribution within the central anomaly probably is a result of the assumption of a uniformly thick magnetized layer being invalid within this region of larger bathymetric relief.

Pacific–Antarctic Ridge—51° S. The relatively uniform spreading on the Pacific–Antarctic Ridge (PAR) for the last 10 My has resulted in some of the best examples of symmetric magnetic anomalies (Pitman & Heirtzler 1966). With the ridge strike of 020°, fast-spreading half-rate of 48 mm/yr and high-magnetic latitude, the resultant magnetic anomalies are exceptionally clear. Bathymetric relief on both flanks of the ridge is minimal with the primary bathymetric change being the gradual deepening of the ocean floor as the crust cools (Sclater, Anderson & Bell 1971).

During expedition Southtow (Mudie *et al.* 1972) a satellite navigated deep-tow profile was taken very close to the Eltanin-19 profile (Pitman & Heirtzler 1966). A traverse of both flanks out to anomaly 3 (Fig. 7) showed that small variations in the spreading rate occur within this 5–My period and that the present centre of spreading is not in the centre of the central anomaly. There is a noticeable long wavelength trend in the magnetization distribution which may be a result of inaccuracies of the IGRF field.

Navigation for the deep-tow profiles was a combination of transponder fixes (Spiess *et al.* 1966), satellite, star, and Loran fixes, and dead reckoning. Within a transponder network the navigational accuracy was usually better than 50 m; outside of this network the deep tow was located with respect to the ship using a cable trajectory computer program (Ivers & Mudie 1973), to an accuracy of about 200 m. During low-speed towing operations the accuracy of the satellite navigation for the ship was 500 m, at its best (Spiess & Sanders 1971), while the Loran and star fixes were good to 2–3 kilometres.

3. Data analysis

Rapid computer analysis techniques have been developed over the last few years to facilitate the interpretation of the near-bottom data in terms of a two-dimensional magnetic source layer. We subtract the IGRF regional field (IAGA 1969) from the data and continue the magnetic anomalies upward onto a level surface, removing

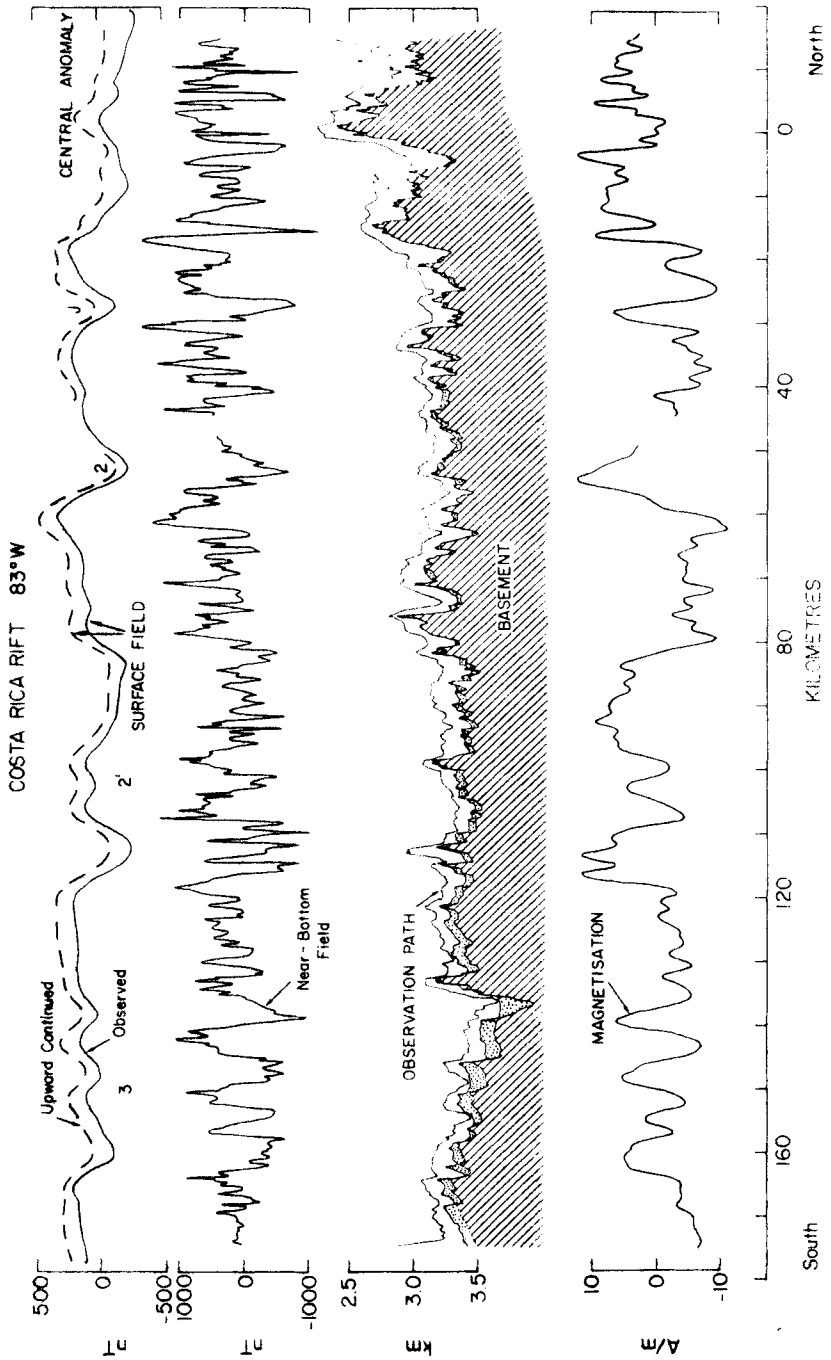

FIG. 6 The near-bottom geophysical profile over the Costa Rica Rift projected along 005°. See caption of Fig. 2 for details.

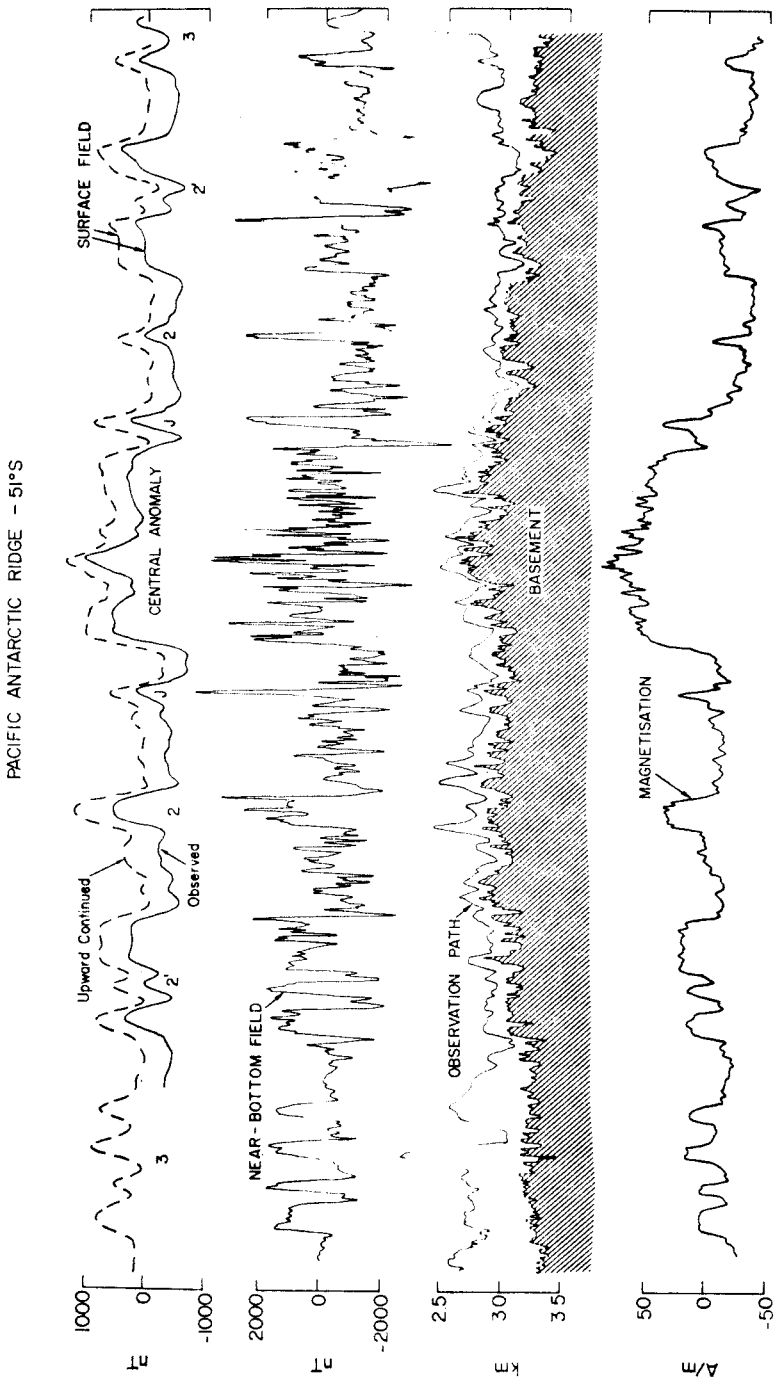

FIG. 7. The near-bottom geophysical profile over the Pacific–Antarctic Ridge projected along 110°. See caption of Fig. 2 for details.

the field variations caused by the changes in the observation depth (Parker & Klitgord 1972). An iterative scheme (Parker & Huestis 1974) is used to invert the values on the level surface in terms of a magnetic layer of constant thickness.

Since detailed near-bottom surveys of portions of mid-ocean ridges (e.g. Larson 1971; Klitgord, Mudie & Normark 1972) and side-looking sonar coverage on traverses of other ridges (e.g. Mudie *et al.* 1972; Atwater & Mudie 1973) have shown that most of the long-wavelength magnetic anomalies and the larger bathymetric relief are lineated parallel to the ridge crest, we assume that the data are two-dimensional and project the profiles onto a plane perpendicular to the strike of the ridge crest. The acoustic basement is used for the upper surface of a 500 m thick layer in which the magnetization is allowed to have only a horizontal variation, determined by the inversion. The direction and magnitude of the regional field are calculated from the IGRF and the axial dipole hypothesis is used to estimate the magnetization direction. The near-bottom magnetic data (Parker & Klitgord 1972) over each ridge crest are continued upward from the uneven track onto a horizontal line about 100 m above the highest point of the observation track. The inversion of magnetic data on the level surface amplifies high and low wave numbers; high and low pass filters with cosine tapers (Schouten & McCamy 1972) were used to reduce the effect of noise at these wave numbers and improve convergence (Parker & Huestis 1974). This inversion is comparable to a downward continuation from the level surface to a level surface approximately midway between the topographic extremes. The distances between these two level surfaces and the filter parameters for each profile are given in Table 1. Wavelengths less than 1 km generally have been attenuated or removed entirely so that the magnetization distributions contain little information about wavelengths under 1 km. This should be compared with the analysis of surface data where it often is necessary to filter out information at wavelengths less than 3 or 4 km to reduce the noise (Bott & Hutton 1970; Blakely & Schouten 1974).

A large amplification of noise also occcurs at the very long wavelengths, introducing unrealistic long-period oscillations in the magnetization distributions (Schouten & McCamy 1972). Diurnal variations and inaccuracies in the regional field are possible sources of noise at wavelengths comparable to the lengths of the survey lines (λ max). The effect of this noise varied on different profiles; on some, it produced a very pronounced long-period (>60 km) oscillation while on others, there appeared to be no need for high pass filtering. Only the Juan de Fuca Ridge, East Pacific Rise and Costa Rica Rift profiles were high-passed with the cosine taper filter (filter parameters are given in Table 1), but in all of the profiles, there are small, apparently spurious long-wavelength oscillations. These make it difficult to choose a zero level for the magnetization distributions; for each of the profiles, the zero level has therefore been chosen so that the mean of the magnetizations is zero.

The magnetizations calculated by this method reproduce the magnetic anomalies with a rms error of less than 1 per cent. The maximum errors from each profile are given in Table 1, along with the peak to peak anomalies in the vicinity of this maximum error. The two largest errors are found on the Galapagos Spreading Centre and the Pacific–Antarctic Ridge, within the region of the central anomaly magnetization high (see Section 5). As an additional check on the inversion method, the observed anomalies on the uneven path from part of the near-bottom profile within the central anomaly on the Pacific–Antarctic Ridge have been compared with anomalies calculated on this path using the magnetization distribution obtained at a 100 m spacing. A magnetized layer model was constructed of adjacent, uniformly magnetized blocks, 0·1 km wide and 0·5 km thick, the upper surface of the model following the basement relief. A standard program, which evaluates the field from each block in elementary function and then sums (Vacquier 1972), was used to calculate the anomalies on the uneven track (Fig. 8). The filtering during the inversion removed much of the information in wavelengths less than 1 km, but the edge effects of the block model

Table 1

Filter parameters for the inversion of the near bottom magnetic data. An estimate of the downward continued distance involved in the inversion is given by DZ. This is the distance between the level surface onto which the original uneven track data had been upward continued and the level surface through the middle of the topographic extremes. The limits for the cosine tapers which were used to low- and high-pass the spectra of the magnetic data are given as λ_{low} and λ_{high}. The wavelengths between $\lambda_{low,\ 1.0}$ and $\lambda_{high,\ 1.0}$ were not affected by the filters and the wavelengths below $\lambda_{low,\ 0.0}$ and above $\lambda_{high\ 0.0}$ were completely suppressed.

	Inversion filtering parameters						
	Juan de Fuca Ridge	Gorda Rise Central	Gorda Rise Flank	East Pacific Rise	Galapagos Spreading Centre	Costa Rica Rift	Pacific–Antarctic Ridge
DX (km)	0·10	0·10	0·10	0·10	0·10	0·10	0·20
DZ (km)	0·69	1·03	0·45	0·63	0·60	1·20	1·04
λ_{max} (km)	204·8	102·4	102·4	204·8	204·8	204·8	419·8
F_{pp} (nT)	3000·0	1200·0	1500·0	1200·0	2500·0	1200·0	2500·0
ΔF (nT)	33·1	23·4	41·9	16·1	194·5	24·2	80·3
$\lambda_{low,\ 0.0}$ (km)	0·7	0·4	0·4	0·5	0·5	1·0	0·4
$\lambda_{low,\ 1.0}$ (km)	1·3	0·9	0·8	1·2	1·2	2·1	0·8
$\lambda_{high,\ 1.0}$ (km)	41·0	102·4	102·4	41·0	204·8	102·4	419·8
$\lambda_{high,\ 0.0}$ (km)	204·8	∞	∞	204·8	∞	∞	∞

DX = Data spacing
DZ = Distance downward-continued
λ_{max} = Maximum wavelength
ΔF = Maximum error in calc. anomalies
F_{pp} = Peak-to-peak anomaly near max. error

$\lambda_{low,\ 0.0}$ = Shortest λ completely suppressed
$\lambda_{low,\ 1.0}$ = Shortest λ completely unsuppressed
$\lambda_{high,\ 1.0}$ = Longest λ completely unsuppressed
$\lambda_{high,\ 0.0}$ = Longest λ completely suppressed

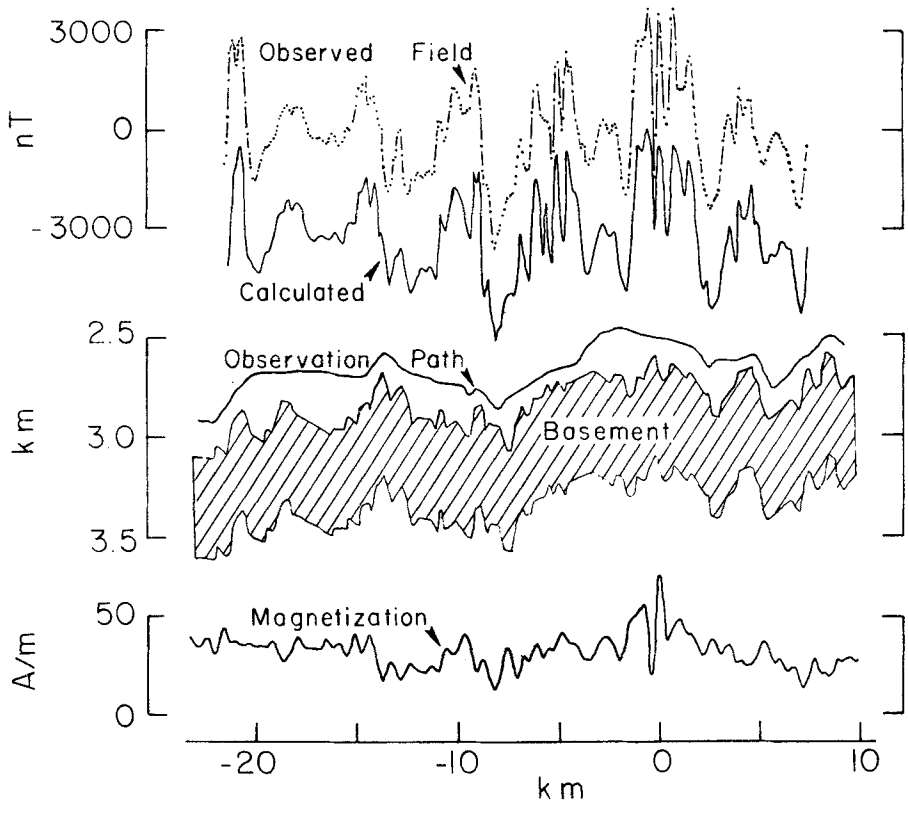

FIG. 8. Comparison of the near-bottom magnetic anomalies (dot-dash curve) from the central anomaly of the Pacific–Antarctic Ridge with the magnetic anomalies (solid line at top) calculated on the observation path (Vacquier 1972), using the 0·5 km-thick magnetized layer whose upper surface is the basement relief. The magnetizations at the bottom were determined by the inversion method of Parker & Huestis (1974). The calculated field has been offset by 3000 nT from the observed field.

introduced components in these shorter wavelengths, resulting in the calculated anomalies appearing to have more high-frequency information than the actual observed anomalies.

4. Reversal boundaries and transition widths

The magnetized layer is created at a spreading centre by extrusive pillow and flow basalts and their associated feeder dikes. If this magnetized layer was formed over a broad zone, then an overlap in magnetic polarities of the basalts would be expected near reversal boundaries, limiting the fidelity with which the magnetized layer records field variations. Atwater & Mudie (1973) concluded from near-bottom data on the Gorda Rise that most of the magnetized layer is formed within 1–4 km of the centre of spreading. The width of this zone depends on the crustal generation process, while it is the actual location that is of interest in determining spreading rates for the ridges and ages of the oceanic crust.

Transition zones are the regions separating normally and reversely magnetized oceanic crust, assuming that one can identify the polarity of the magnetization of the crust. The uncertainty in the long-wavelength component of the solutions has no significant effect on the determination of the locations of transition zones; the zero levels on Figs 2–7, however, do not separate normally and reversely magnetized crust, and the places where the magnetizations cross the zero level are not necessarily reversal transition zones. Reversal boundaries were located on the profiles by comparing the magnetization patterns with the pattern of magnetic anomalies given by Talwani, Windisch & Langseth (1971) for the last 6 MyBP. The ' box car ' shaped pattern and small short-wavelength (<3 km) fluctuations made the identification of reversal boundaries very easy for crust older than 3 MyBP. The high frequency content increased in the calculated magnetizations for younger crust, but on most of the ridges, the ' box car ' patterns still could be seen and their boundary locations identified. These short-wavelength variations, however, obscured the locations of the boundaries for anomaly 2 on the Juan de Fuca Ridge (Fig. 2) and for the Jaramillo event and the edge of the central anomaly on the Costa Rica Rift (Fig. 6). In these cases where it was not obvious which of the magnetization peaks represented a particular event or reversal boundary, the surface magnetic data were used to help locate the boundary positions. At most of these reversal boundaries, a relative zero level could be determined by assuming that the average magnetization on each side of the boundary should have the same magnitude, but opposite directions. The average magnetization was estimated from a mean level through the high frequency oscillations in the magnetizations within about 10 km of the boundary. With short events, such as the Kaena and Mammoth reversed events within anomaly 2′, the smoothing of the magnetization due to the intrusion process substantially reduced the amplitude of the peaks and troughs in the magnetization, so that it was not valid to assume that the zero level was mid-way between the average magnetizations on both sides of a reversal boundary. In these cases, the zero levels were estimated from the relative zero levels of the adjacent reversals. The horizontal locations of these levels were assumed to be the locations of the reversal boundaries to be used in the calculation of spreading rates and boundary ages (see Section 7). There are some errors associated with assigning these positions to be the reversal boundary locations, but the average transition widths of about 2 km (see below) imply that this choice probably has an error of less than ± 1 km.

The widths of the transition zones at the reversal boundaries can be estimated from the magnetization distributions even though there is some uncertainty produced by the short-wavelength content near the reversals. Using the arbitrary definition of the transition zone as the narrowest zone in which 90 per cent of the magnetization transition occurs (Atwater & Mudie 1973), the transition widths for the six different ridges ranged from 1 to 6 km (Fig. 9). This lower limit of 1 km is an artifact of the filtering in the inversion, but the distribution of the boundary widths greater than 1 km indicates that very few boundaries would be expected to have a width less than 1 km. There are too few boundaries in the GSC data to be conclusive, but the transition widths for the other five ridges are distributed about a central value of 2–2·5 km for the CRR, the GR, the EPR and the PAR and about 3 km for JFR. Since these widths are greater than the filtered wavelengths, they probably give a good estimate of the average half-width of the zone of formation. The transition widths do not appear to vary much with age or from ridge to ridge, although the spreading half-rates range from 30 to 50 mm/yr. This suggests that for fast spreading ridges, the width of the zone of formation is not very sensitive to spreading rate variations.

The detection of short events is difficult with near-bottom marine magnetic data because of this smoothing of the magnetic record. There is a general noise level in the calculated magnetizations at wavelengths of less than 2 or 3 km; this noise level may be a result of errors in the model for the magnetized layer and real variations in the

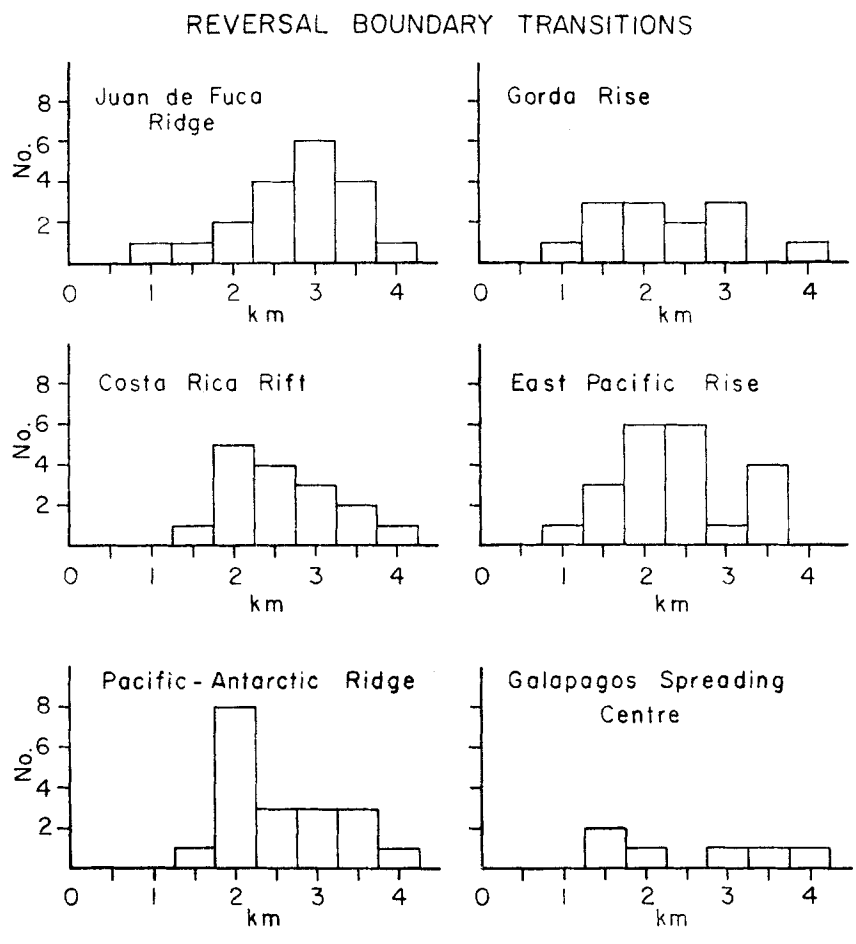

FIG. 9. Histograms for the widths of the transition zones of the magnetic field reversals recorded in the magnetized crust of each of the ridges traversed with deep tow. The width of a transition zone has been arbitrarily defined as the narrowest zone in which 90 per cent of the magnetization transition occurs (Atwater & Mudie 1973). One transition width of 5 km for the East Pacific Rise and one of 6 km for the Costa Rica Rift are not shown.

magnetization. To be detected, a short event must produce a magnetization peak which is greater than this level on several ridges. Events with a duration of less than 10 000 yr are obscured by the noise on the PAR, and they would have to be longer than about 20 000 yr on the slower spreading ridges, assuming a half-width of about 2 km for the zone of formation. This implies that the 10 000 yr duration probably is a lower limit for the field changes which could be detected with this set of near-bottom data.

5. Variations in amplitude of magnetization

The magnetization of ocean crust has a variable magnitude as well as the directional change caused by reversals of the geomagnetic field. Chemical differences in the crust, and spatial and temporal variations in the geomagnetic field produce magnitude differences in the magnetization from place to place within the oceanic crust. The

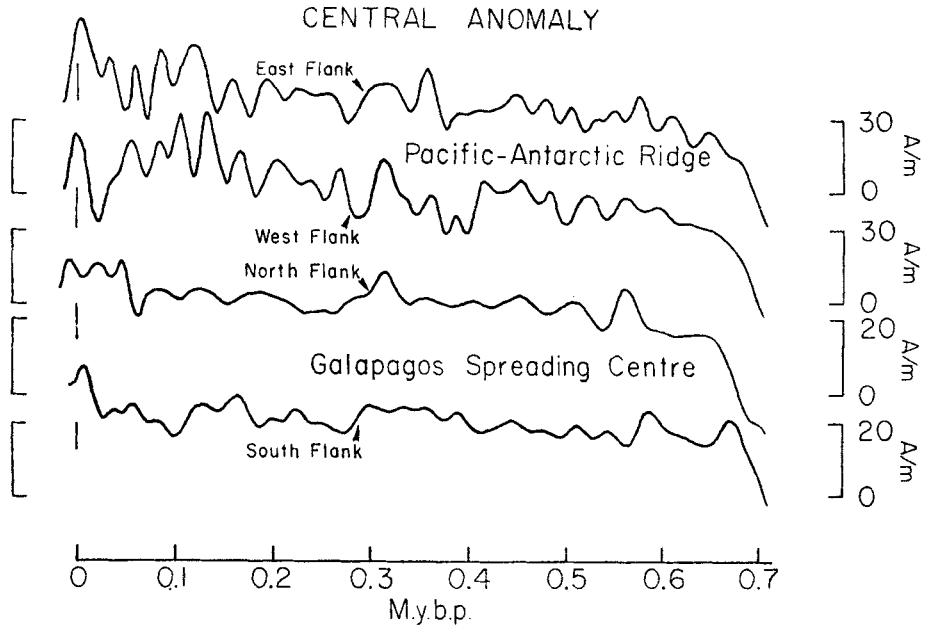

FIG. 10. The magnetization as a function of age on both flanks of the Pacific–Antarctic Ridge and the Galapagos Spreading Centre. The short-wavelength variations are necessary to fit the observed fields, using the 0·5 km thick layer and the bathymetric relief.

change in the magnetic field with magnetic latitude is the major cause of these magnitude differences between segments of the oceanic ridge system (Schouten 1971), although chemical differences are also important on the Juan de Fuca Ridge (Kay, Hubbard & Gast 1970) and on the Galapagos Spreading Centre (Anderson *et al.* 1975). Time varying changes in the magnitude of the geomagnetic field could produce some short-wavelength fluctuations (<3 km) on the flank of a ridge, but most of the magnitude variations probably are caused by chemical changes produced by differences in magma sources, cooling history of the basalts and the extent of weathering.

The magnetizations determined for the six deep-tow profiles have a short-wavelength fluctuation (<3 km) superimposed upon the large variations produced by reversals of the magnetic field. Over some portions of the oceanic crust the calculated magnetizations show only a small amount of high-wave number variability (e.g. the Juan de Fuca Ridge, Fig. 2; The Galapagos Spreading Centre, Fig. 5; the Pacific–Antarctic Ridge, Fig. 7) and reversals of the magnetic field have produced the classical 'box car' shapes in the magnetizations. The short-wavelength magnitude variations in these regions can be seen most clearly within the central anomaly (Fig. 10). The fluctuations do not appear to be coherent between the two ridges or the two flanks of the same ridge, indicating that they probably were not caused by oscillations in the geomagnetic field. Chemical differences could cause some of these variations, but more likely sources are small deviations of the actual magnetized layer from our uniform thickness model. In some places the short-wavelength variations are more apparent in the magnetizations, at times obscuring the reversal boundaries. This is very noticeable around the central anomaly of the Gorda Rise (Fig. 3) and the Costa Rica Rift (Fig. 6) where there is large bathymetric relief. Errors in our model for the magnetized layer again are a likely source of this variability since the effects of the magnetization of the bottom of the magnetized layer are more important when the bathymetry has about the same scale of relief as the thickness of the layer. In general,

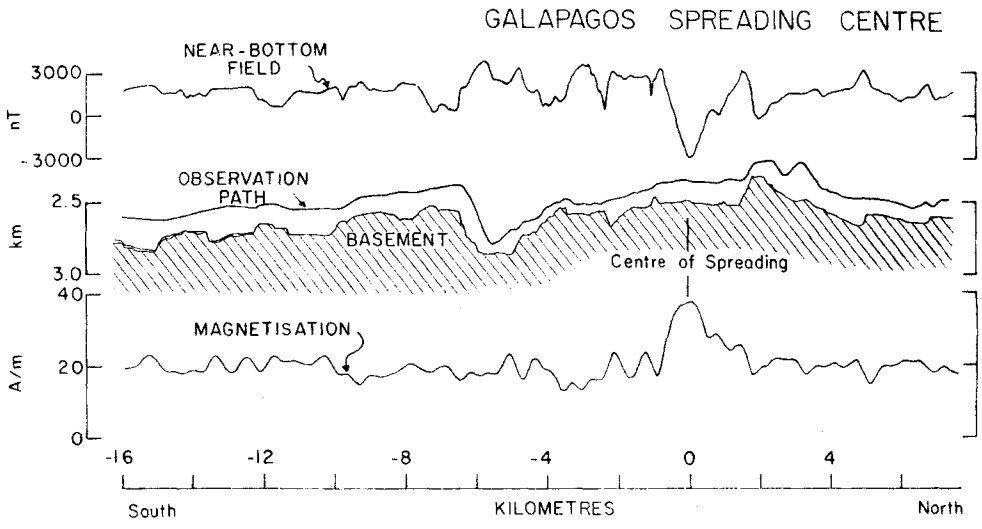

FIG. 11. The magnetization high within the central anomaly over the Galapagos Spreading Centre.

this uncertainty in our model of the magnetized layer prevents us from making any reliable statements about the existence or causes of very short-period magnetization changes, including the possibility of fluctuations in the amplitude of the geomagnetic field.

There is a narrow region with very high magnetizations within the central anomaly of the Gorda Rise (Fig. 3) (Atwater & Mudie 1973), the Galapagos Spreading Centre (Fig. 11) and the Pacific–Antarctic Ridge (Fig. 7), an effect also found by Irving *et al.* (1970) in a suite of dredge samples from the Mid-Atlantic Ridge. These regions have widths of 6 km, 2 km and 10 km respectively, with magnetizations reaching 30–40 Å m^{-1}. The large magnetic anomaly produced by the magnetization high was observed on five of six crossings of the central anomaly on the Galapagos Spreading Centre (Fig. 12) and it appears to be associated with a small ridge of fresh pillow and flow basalts. The long near-bottom traverse of this spreading centre (Fig. 5) had only a slight indication of the magnetization high over this same small ridge, indicating the variability of the magnetization. Dredge samples of pillow basalts from the Galapagos Spreading Centre have an anomalously high iron content (Anderson *et al.* 1975), but the magnetic anomaly pattern suggests that all of the magnetized high within the central anomaly is superimposed on top of this general high level of magnetization on the Galapagos Spreading Centre. Both the magnetization high and the small ridge on the Galapagos Spreading Centre are elongated parallel to the sea-floor spreading magnetic anomaly lineations and encompass the centre of spreading as determined from the sediment distribution and the symmetry of the sea-floor spreading anomalies (Klitgord & Mudie 1974). The regions of high magnetization on the Gorda Rise and Pacific–Antarctic Ridge are offset slightly from the centre of the central anomaly, but the almost complete lack of sediments within these regions indicates that they are probably very young. This magnetization high was not seen on near-bottom traverses of the East Pacific Rise at 21° N (Larson 1971) or on the Costa Rica Rift (Fig. 6) suggesting that not every spreading centre produces such a feature or that it only occurs episodically. Surface ship magnetic profiles over many, but not all, segments of the oceanic ridge system clearly show a magnetization high within their central anomaly (Klitgord 1975) indicating that it is a common feature of the younger crust of many spreading centres.

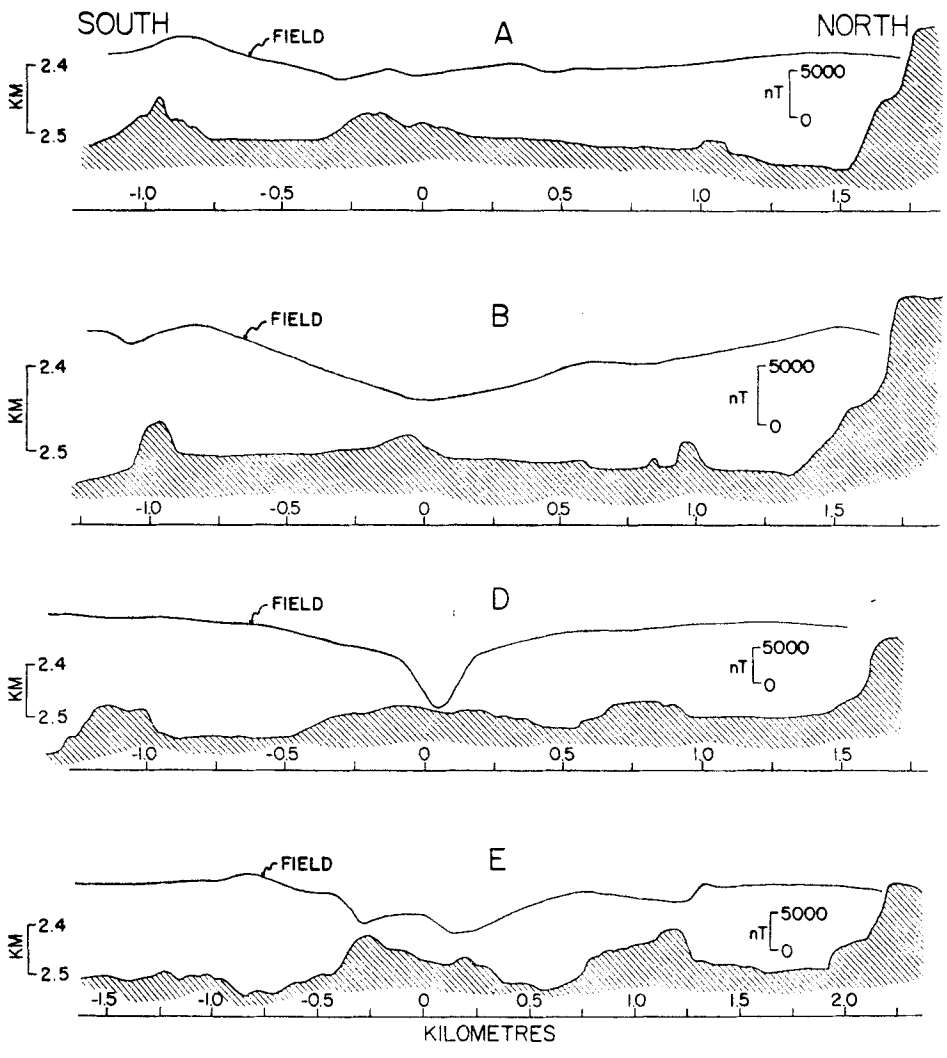

FIG. 12. Line drawings of the original near-bottom bathymetric records from four tracks across the central 4-km region of the Galapagos Spreading Centre (Klitgord & Mudie 1974) (vertical exaggeration = 2:1). The distances are in km from the centre along the track and not projected. The large troughs in the magnetic field profiles indicate the location of the magnetization high on each crossing. The large scarp of the ridge-crest block is seen at the right on each profile.

The large average magnetization of fresh pillow basalts can explain this peak in the magnetization. A study of the magnetic properties of a large, fresh pillow basalt has shown that the pillow has a large variation in magnetization with depth below its cooling surface (Watkins, Paster & Ade-Hall 1970). Beneath the glassy outer rind there is a highly magnetized variolitic layer which is only 10–20 mm thick, while the rest of the interior of the pillow has a weaker magnetization. This variation in magnetization with depth within a pillow was associated with the changes in titanomagnetite content and the increase in grain sizes with depth, since the smaller crystals are more highly magnetized than larger crystals and the slower cooling portions of a pillow develop larger crystals (Marshall & Cox 1972). The outer, variolitic zone had a very small grain size and a high titanomagnetite content. Further

towards the interior of a pillow there was a small decrease and then an increase in the titanomagnetite content, but there was a large increase in grain sizes, producing a very large decrease in the magnetization of the interior of a pillow (Watkins *et al.* 1970). Although the small grain sizes of the titanomagnetite are an important source of the high magnetizations within portions of some pillow basalts (Watkins *et al.* 1970), an increase in the titanomagnetite content of the basalts also could produce the higher magnetizations. It probably is a combination of these two properties, grain size and iron content, which controls the magnitude of the magnetization high on any particular ridge.

A decrease in the magnetization with distance from the centre of spreading (Fig. 13) is found on all six of the ridges surveyed with the deep tow; it is a rapid decrease near the magnetization high and a gradual one on the flanks of the ridge. The magnetization magnitudes were determined at each reversal boundary by using the method described in Section 5 to find the zero level. The average magnetizations were estimated over a 10 km wide region on both sides of the reversal boundary and the magnitude was taken to be one-half of their differences; that is, it was assumed that both the normally and the reversely magnetized crust of about the same age on a ridge should have the same magnitude of magnetization. The high wave number content of the magnetization distributions produces some scatter in these measurements, as indicated by the error bars (Fig. 13), but this does not obscure the decreasing trend away from the centre. The different levels of magnetization on the Gorda Rise, East Pacific Rise, Costa Rica Rift and the Pacific–Antarctic Ridge result from

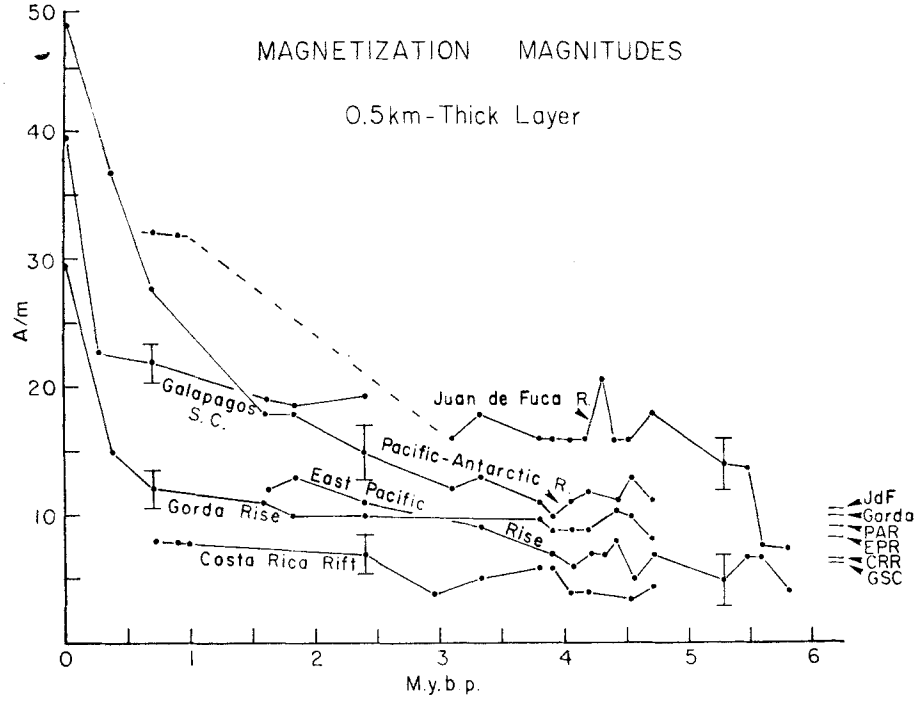

FIG. 13. The magnitudes of the magnetizations as a function of age on the six near-bottom profiles, determined at each reversal boundary assuming that both the normally and reversely magnetized crust have the same magnitude. The error bar on each curve gives an estimate of the error in determining the magnitude. The effect which the variation in latitude has on the magnetizations of the different ridges is indicated at far right, assuming a magnetization of 10 A m^{-1} for the Gorda Rise.

their different magnetic latitudes, while the higher levels for the Galapagos Spreading Centre and the Juan de Fuca Ridge may be caused by the higher iron content in their basalts (Anderson *et al.* 1975; Kay *et al.* 1970).

Weathering of the basaltic layer can account for both the rapid and the slow decreases in magnetization. Marshall & Cox (1971, 1972) have shown that as weathering progresses towards the interior of a pillow basalt, titanomagnetite is oxidized into the less magnetic titanomaghemite. The basalts, discussed by Marshall & Cox (1972) in their explanation of the slow decrease in magnetization of the flanks, already had weathered beyond the highly magnetized variolitic layer; therefore they probably were looking at the weathering of the larger grains in the interior of the pillow. The same oxidation reaction also should affect the highly magnetized variolitic zone. Since the grains are much smaller in this outer zone, there is a greater surface for the weathering to act upon, and the oxidation probably progresses much more rapidly through this zone than at the rate described by Marshall & Cox (1972) for the interior of the pillow. This very rapid oxidation of the highly magnetized variolitic zone could account for the very narrow zone within which the magnetized highs are found on oceanic ridges. The effect also is enhanced because the variolitic zone, even though it is only 10–20 mm thick, represents a substantial fraction of the volume of a pillow. The ages of the crust covered by these high magnetization zones suggest that the weathering of the variolitic layer in the pillow basalts takes place in less than 100 000 yr on the Pacific–Antarctic Ridge, and less than 30 000 yr on the Galapagos Spreading Centre. Since new material probably flows several kilometres from where it is extruded (Atwater & Mudie 1973), these times are only upper estimates. This requires a rate of weathering which is 4 or 5 times greater than that found by Marshall & Cox (1972) for a pillow from the flank of the Juan de Fuca Ridge, but this could be reasonable since the grain sizes increase by a factor of 2 or 3 towards the interior of the pillow (Marshall & Cox 1971), which means over 4 or 5 times more surface area to be affected by weathering in the variolitic zone. Thus, the weathering of the variolitic zone could produce the narrow region with the magnetization high, while the weathering of the rest of the interior of pillows could produce the gradual decrease in magnetization on the flanks.

6. Topographic effects and the magnetized layer

The short-wavelength (<3 km) magnetic anomalies observed above the ocean floor are produced by several possible effects, including variations in the magnetization of the basalts, effects of the bathymetric relief and variations in the observation depth. The first two possibilities are of the most interest because they reflect changes in the magnetized layer. The variations of magnetization were discussed in the previous section, with the effects of the bathymetry and the observation path variations removed. Studies of the bathymetric effects with the observation path variations removed (Miller, Klitgord & Mudie 1974) have indicated that a substantial amount (>30 per cent) of the signal at wavelengths of less than 3 km is associated with the bathymetric relief. In this section, we shall look at the effects which the bathymetric relief has on the short-wavelength anomalies by using a uniformly magnetized layer. If the effects of the variations of the observation path were removed by upward continuation onto a level surface, a substantial attenuation of the very short-wavelength content (<1 km), would make it difficult to visually demonstrate the effects of the uniformly magnetized bathymetric relief. Instead, we have examined the effects on the actual observation path since the desired results are the estimated magnetizations of the smaller bathymetric features and not the separation of the bathymetric effect (those anomalies which would disappear if there were no relief) from the effects of the observation path variations.

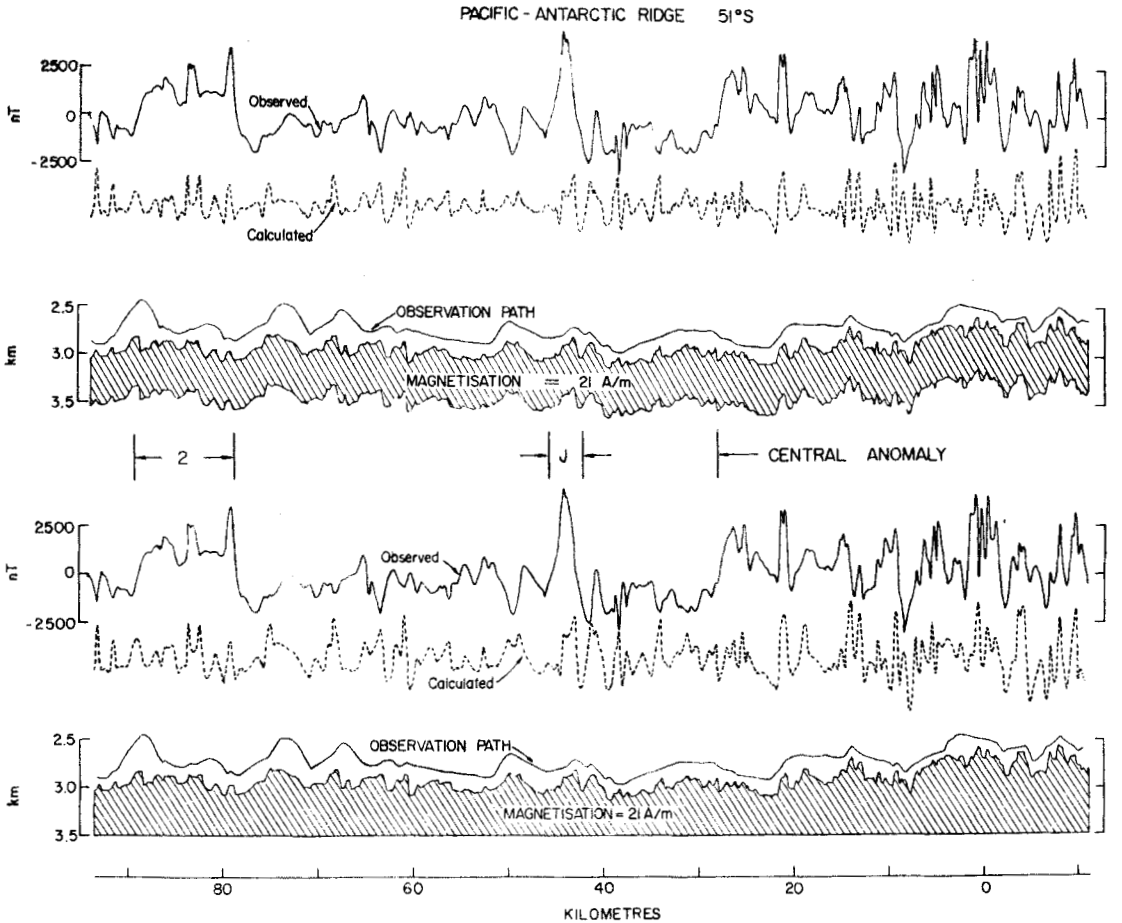

FIG. 14. The effects of the bathymetric relief and a uniform magnetization for (a) a 0·5 km constant thickness model; (b) a flat-bottom model. The near-bottom observed anomalies were taken on the observation path and the method of Vacquier (1972) was used to calculate the synthetic anomalies on the same track.

The short-wavelength content which is not produced by variations in the magnetization of the basaltic crust can be seen in Fig. 14. A comparison of the observed magnetic anomalies with the anomalies produced by a uniformly magnetized layer whose upper surface is the acoustic basement, indicates that the bathymetric relief and observation path variations produce significant small-scale anomalies, but that for the model, short-wavelength magnetization variations are also necessary. The non-uniqueness of potential field-source determinations requires the use of additional assumptions to limit the set of possible models for these short-wavelength anomalies. We shall look at a few reasonable assumptions and discuss the validity of the conclusions which can be drawn from them concerning the magnetization of the layer.

The magnetization usually is assumed to be a constant with depth within a magnetized layer of finite thickness. Studies of land outcrops presumed to be fragments of the oceanic layer, such as the Troodos Massif on Cyprus (Moores & Vine 1971), have shown that at the top of the layer there are a few hundred metres of highly magnetized pillow basalts overlying a more weakly magnetized dike complex. Within this pillow layer, however, there is an increasing percentage of feeder dikes with depth (Gass & Masson-Smith 1963) and, since the pillows are more highly magnetized than the dikes (Marshall & Cox 1971), this results in a decrease in magnetization with depth. Although a vertical variation could have been used in the inversion, a uniform magnetization with depth has been used because it is a simple assumption and the true variation with depth is not known. This choice of the vertical variation affects the amplitudes of the magnetizations, but it has very little effect on the relative horizontal variations (Parker & Huestis 1974). Even if we have not estimated the magnitude correctly, the effect on the spacing of the magnetic reversals is negligible.

The assumption of a uniform horizontal distribution of magnetization for the upper layer of oceanic crust has been used with surface-ship data (Talwani *et al.* 1971) and near-bottom data (Atwater & Mudie 1973), to determine the magnitude of magnetization of bathymetric features. Again, the assumption must be made about the vertical extent of the magnetized layer since the depth to and shape of the bottom of the magnetized layer affects the amplitudes of magnetic anomalies. The use of a flat bottom to the layer (Fig. 14(b)) (e.g. Talwani *et al.* 1971) involves the assumption that the bathymetric relief was being formed as the magnetized layer was formed; the highs and lows on the ocean floor represent excess or deficient amounts of magnetized basalt which had been added to a layer with a constant bottom depth. This may be valid for the small bathymetric relief, but near-bottom studies of slow- and fast-spreading ridges (Atwater & Mudie 1968; Klitgord & Mudie 1974) have shown that the larger relief was produced by block faulting after most of the magnetized layer had been formed. The use of a model with a uniformly thick magnetized layer (Fig. 14(a)) would seem more appropriate for this relief, since the faulting would offset the bottom of the layer as well as the top of the layer. The two synthetic profiles in Fig. 14 show that with near-bottom data, the two models are almost indistinguishable for layer thickness greater than 400–500 m and that only slightly higher magnetizations are required for the 500-m-thick layer to produce the same anomalies as the flat-bottom layer. If one knows for certain that bathymetric peaks are uniformly magnetized, then it would be possible to put a lower limit on the magnetization needed within the peaks to produce the observed anomalies.

The magnetic anomaly profiles in Fig. 14 show that with either model, horizontal variations in the magnetization are needed to reproduce the magnetic anomalies, even within crust which was produced when the polarity of the field remained the same. This severely limits any conclusions which can be drawn from uniform magnetization modelling, since, for a given topography, there exists a horizontal distribution of magnetization, called the magnetic annihilator (Parker & Huestis 1974), that will produce no external magnetic field. Any scalar multiple of the annihilator can be added to the magnetization without changing the resulting field. Since the annihi-

lator has a non-zero mean, the magnitude of the magnetization and its horizontal variation can be varied arbitrarily much by adding a multiple of the annihilator. The oceanic crust which forms the large bathymetric features probably was generated over a long period of time at the spreading centre and can be expected to have recorded a rather variable field, including reversals. With these features, the results of uniform magnetization studies are very tenuous. Chemical variations will cause some smaller peaks to be more highly magnetized than others, but only small amounts of variation are reasonable within a given small feature and the uniform magnetization assumption is fairly reliable.

Information about the magnetized layer can be learned from the short-wavelength anomalies despite the ambiguities introduced by the magnetic annihilator. The regions of normally and reversely magnetized crust are indicated in Fig. 14 by the places where there is a strong correlation or anticorrelation between the magnetic anomalies. The magnetic anomalies associated with the smaller bathymetric features indicate that a magnetization of 20–25 Å m^{-1} is needed within the central anomaly to reproduce them with topographic anomalies. In the region of the magnetization high ($\sim$0 km, Fig. 14) even higher magnetizations are required. Allowing a reasonable amount of horizontal variation from the annihilator introduces an uncertainty of ± 5 Å m^{-1} to this estimate of the magnetization. The magnetizations are about the same as those determined by the inversion of the deep tow data using a 500 m thick layer (Fig. 7), indicating that 500 m $\pm$ 150 m would be a reasonable estimate for the layer thickness. There is a decrease in the short-wavelength content of the field on the flanks of the Pacific–Antarctic Ridge (Fig. 7) which corresponds, roughly, with the amplitude decrease in the magnetizations and it probably is caused by the weathering of the basalt layer. Scarps form the edges of many of the bathymetric highs and they appear to be unsedimented (Mudie *et al.* 1972), allowing the weathering to continue fairly rapidly, even on the flanks, reducing the bathymetric effects of the edges of the features.

7. Spreading rate variations and asymmetric spreading

Poles of relative motion cannot remain fixed with respect to their plate pairs when large angular motion takes place in a system of more than two plates (Le Pichon 1968). Thus changes in direction, and probably velocity, may be common on ridges that have produced 1000 km of crust or more (about 10°). Our investigations have been almost entirely confined to velocity variations, as we shall see, but it is quite unlikely that the accelerations we find were not accompanied by slight shifts in pole positions. We discover that in the Pacific the accelerations occur discontinuously with a frequency around once every million years and that almost perfectly constant rates prevail between the discontinuities. Although movement of the poles of motion is inevitable on kinetic grounds, geometry alone cannot tell us the way the motion will occur, how fast or when (McKenzie & Parker 1974). Perhaps the shifts are more likely to happen at times when other dramatic alterations occur in the plate configuration (e.g. the disappearance of a plate or the collision of two continental plates) and it is quite possible that such events may effect ridges at great distances; however, the number of velocity jumps we observe is so large that it is very improbable that every one is connected with a major rearrangement elsewhere. The velocity adjustments occurring at about 3 My (and perhaps at 5 My) in the majority of our ridges may be an example of a response to a large scale perturbation in the plate pattern. In the following paragraphs we give a detailed analysis of the spreading rate variations that we have discovered and collate other relative studies on directional shifts found in the Pacific and Atlantic.

To find accurate spreading rates when the geomagnetic time scale is poorly known we determine the ratio of velocities, which can be done with rather high

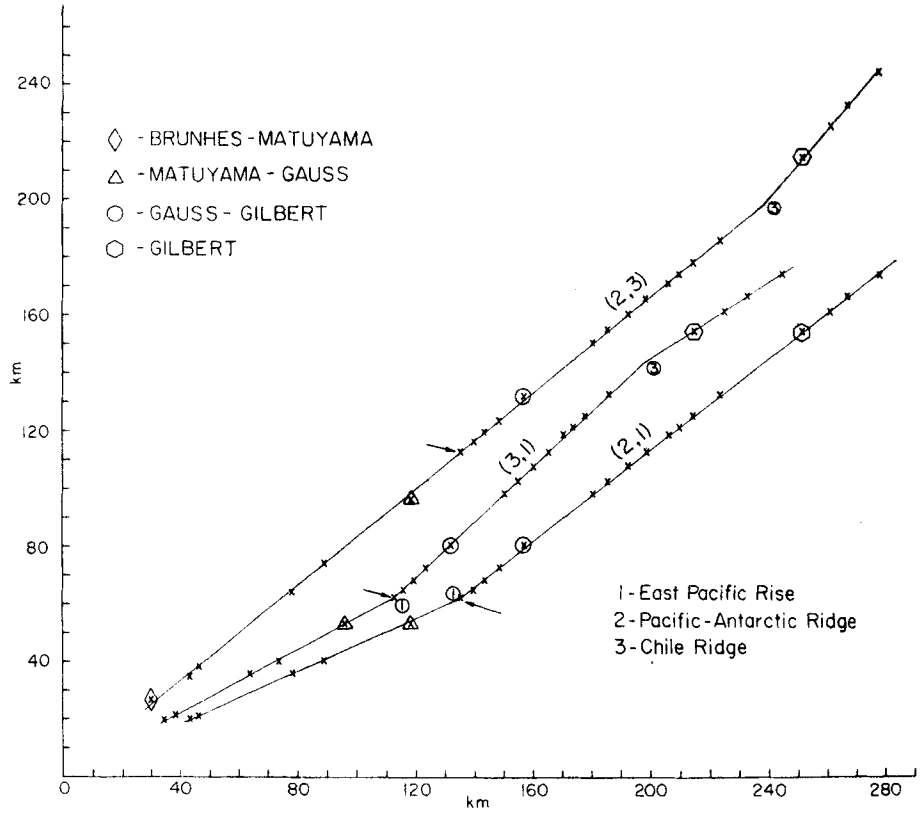

FIG. 15. The distance *vs* distance graphs for the reversal boundaries on different pairs of three ridges. The numbers in parentheses (A, B) refer to the pair of ridges, with ridge A along the *X*-axis and ridge B along the *Y*-axis. Epoch boundaries are shown by the symbols listed in the upper left corner. A set of reversal boundaries of the same age are shown by arrows and the circled numbers refer to the ridge which changed spreading rate.

precision. On each of the surveyed ridges it is possible to pick the position of a particular reversal, thus establishing the amount of crust created on each ridge since that time. Suppose that, for a pair of ridges, we plot the distances from the rise crest to a whole sequence of reversals on one ridge against the corresponding distances on the other. As can be seen in Fig. 15, a remarkable thing happens: the points lie very accurately on a series of connected straight lines. This immediately implies that the ratio of velocities on the two ridges remains constant, where the points lie on a particular line, but it changes abruptly where the slope changes. The slope of the straight line gives the ratio of velocities directly.

It is conceivable that, on the straight parts of such a plot, the absolute spreading rate of both ridges was varying, the changes in one keeping exactly in step with those in the other in order to maintain a fixed ratio. This seems altogether rather unlikely and we propose that it is much more probable that, during the periods of constant velocity ratio, the absolute values of spreading rate were constant individually.

Let us now turn to the times when abrupt accelerations occur: from a single pair of ridges it is not possible to say whether both ridges changed velocity, or only one did. However, when a third ridge is brought into the picture, a decision can almost always be made. In Fig. 15, the time of the first break of 1 against 2 is indicated by an arrow; we find a similar break at that time in 1 against 3 but not in 2 against 3. From our hypothesis that when the ratios remain constant, the velocities of the individual plates are also constant, it follows that ridge 2 (the Pacific–Antarctic Ridge) did not alter its spreading rate at that time and therefore that only ridge 1 (the East Pacific Rise) underwent an abrupt acceleration. This identification can be verified by introducing yet another ridge and plotting 2 against it; if no break in slope occurs at the time when the 1–2 change took place, we confirm that ridge 1 was responsible for the slope change.

The process outlined above has been carried out with all possible ridge pairs; the very high accuracy to which the points fall on straight lines in our example is a universal feature of all the plots. In order to get some idea of the precision, least-squares fits were performed on the various sections. Simple regression cannot be used here because, of course, both ordinate and abscissa exhibit variance. We assumed that navigational error was chiefly responsible for the misfit and estimated the precision of the position determinations from the type of navigation in use. Now we were able to use a regression analysis in which the ratio of the x and y standard errors was assumed (Kendall & Stuart 1967). The standard errors were assigned as follows: satellite navigation with slow steaming ± 1 km; with fast steaming ± 2 km; all other navigation ± 3 km. The computed standard error for an observation point resulting from the regression analysis was almost always less than 2 km, the only exceptions occurring when the straight line segment was very short. The estimated standard error of the slopes of the segments was typically 2 or 3 per cent; these errors were combined in the usual way for independent estimates when the slope ratios were computed and these are the error figures given in Fig. 16 for the ratios.

Because the breaks in the line segments are so obvious in every case, we did not write an elaborate program to find the optimum unbiased division between regimes of constant velocity. Even when several ridges appeared to accelerate at about the same time (at about 3 MyBP and 5 MyBP) we could always find at least one pair that plotted on a straight line during the disturbed period.

To convert the ratios of velocities into absolute values (Fig. 16) we took three radiometrically dated geomagnetic reversals as benchmarks, the Brunhes–Matuyama boundary at 0·70 MyBP (Dalrymple 1972), the Matuyama–Gauss boundary at 2·41 MyBP (McDougall & Aziz-Ur-Rahman 1972) and the Gauss–Gilbert boundary at 3·32 MyBP (Dalrymple 1972). The errors in absolute velocities are larger than those in the ratios because of the additional (statistically independent) errors in the age determinations.

Our near-bottom profiles, usually acquired over only one flank of each ridge, were supplemented by additional surface magnetic profiles on the other flanks to help distinguish between rate changes and asymmetric spreading. Velocities on the East Pacific Rise at 21° 10′ N (Larson 1972) and on the northern flank of the Costa Rica Rift (Grim 1970) were found from their magnetization distributions (Fig. 17), as described above. The composite profile over the Juan de Fuca Ridge (Vine 1966) was used for the western flank, but since no bathymetric data were available, the magnetization was not calculated. High latitude anomalies, however, are only slightly skewed (Schouten 1971) so the reversal boundary locations were estimated from the anomaly profile. The spreading rates calculated from these surface profiles are given in Fig. 18. The Eltanin-19 profile was the only one available over a long portion of the east flank of the Pacific–Antarctic Ridge at 51° S, and, since it is also at a high latitude, reversal boundaries were located from the anomaly profile. The motion on this flank appears to be quite variable, so spreading rates were not calculated but

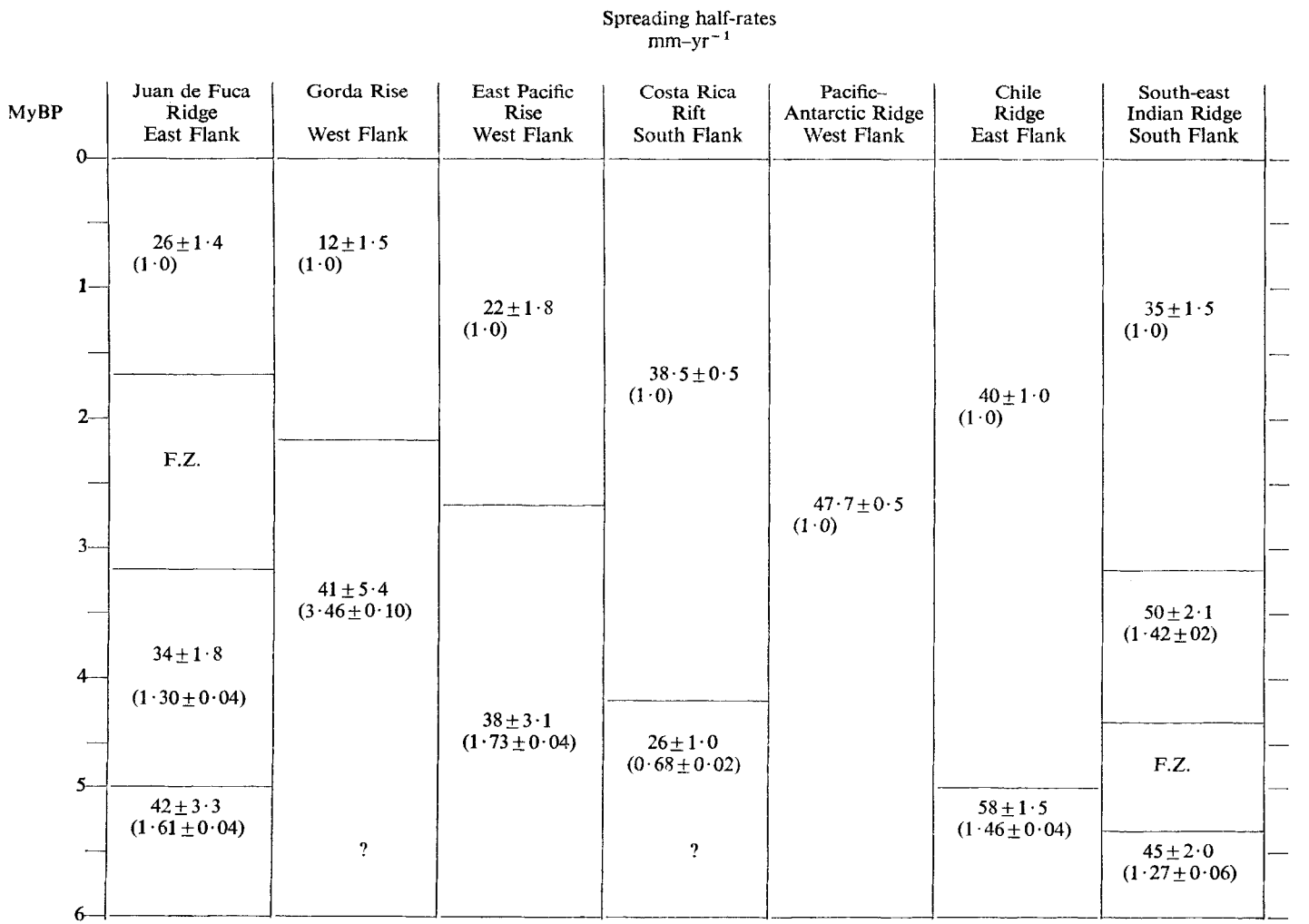

FIG. 16. Spreading half-rates and standard errors from near-bottom profiles for the ridge flanks used in the calculation of a revised geomagnetic time scale. The ratio of the spreading half-rates to the present half-rates are given in parentheses.

only plotted in Fig. 19(a) for comparison with the deep tow profile. Fig. 19 shows distance *vs* age graphs for all these ridges, as well as differences between observed distance to reversals and those calculated using half-rates and the time scale from this paper.

To determine velocities accurately, shifts in direction must be accounted for. Large changes in relative pole position can be seen in the lineation pattern of magnetic anomalies and fracture zones (Menard & Atwater 1968). Smaller ones are harder to detect because there are few regions which are surveyed on a scale fine enough to define small differences in lineation trends. We shall ignore small direction changes since they produce only minor errors in spreading rate calculations.

Spreading may have altered direction between 4 and 7 MyBP on the Juan de Fuca Ridge and Gorda Rise (Menard & Atwater 1968; Elvers *et al.* 1973). The magnetic lineation pattern in the north-east Pacific (Raff & Mason 1961) indicates, however, that this mainly took place before 6 MyBP. On the eastern flank there is no significant change on the Juan de Fuca Ridge from 0 to 6 MyBP. The crust east of the Gorda Rise is very fractured and a profile across it has not been included. Morgan, Vogt & Falls (1969) suggest a rotation of the East Pacific Rise between 8 and 10

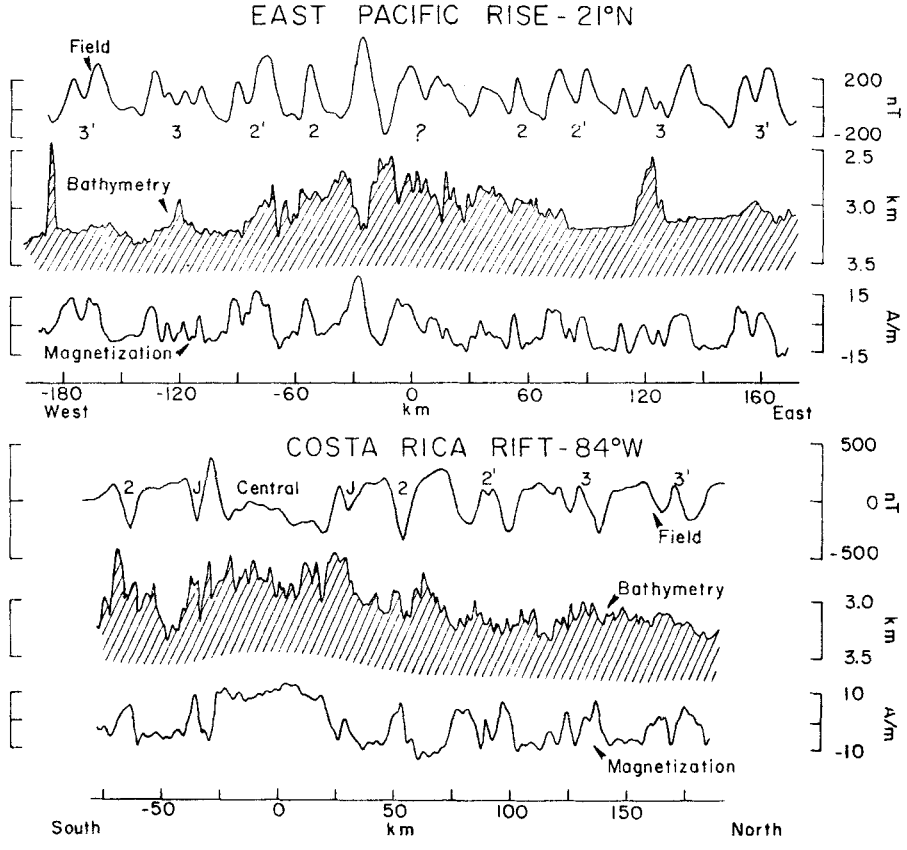

FIG. 17. Surface ship geophysical profiles over the East Pacific Rise and the Costa Rica Rift. The East Pacific Rise profile is from the Scripps Institution of Oceanography cruise GAM-II (Larson 1972) and the profile over the northern flank of the Costa Rica Rift is from the OCEANOGRAPHER–69 Cruise (profile E of Grim 1970).

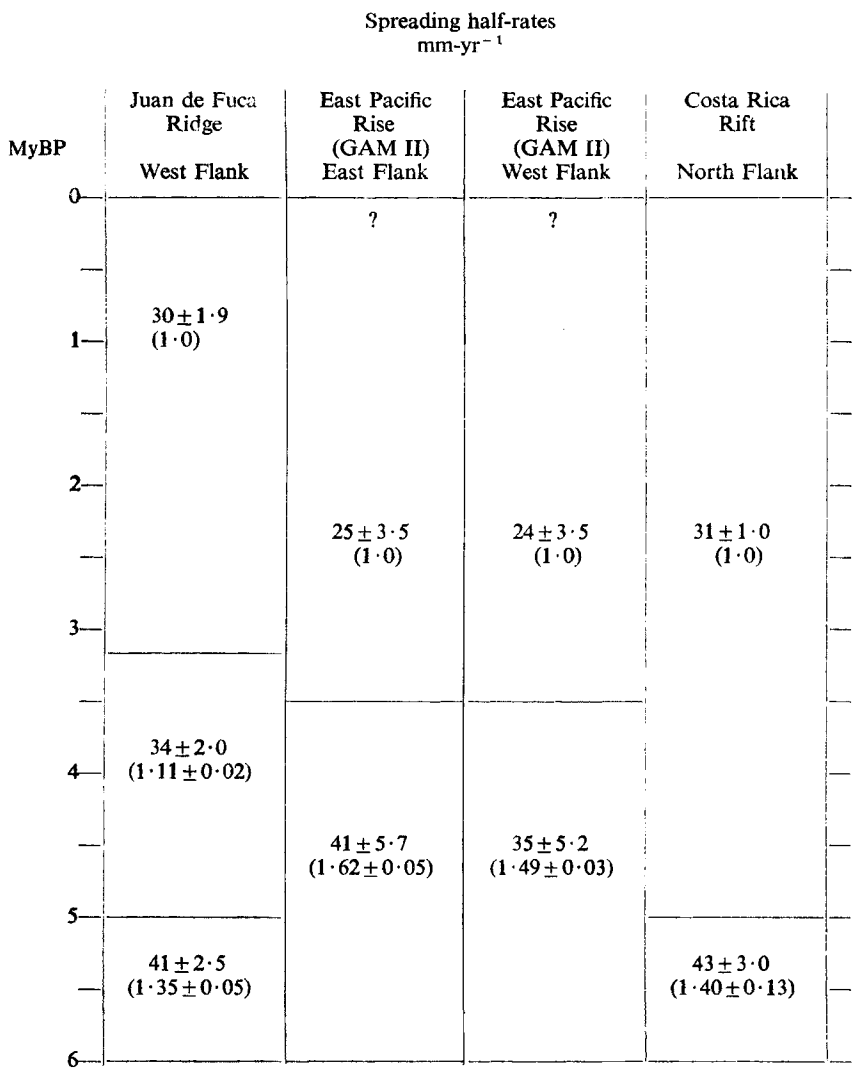

FIG. 18. Spreading half-rates and standard errors for the ridge flanks traversed by the additional surface ship profiles.

MyBP, but the anomaly pattern at 22_0 N shows a constant lineation orientation for at least the past 6 My (Larson 1972). Data from the northern flank of the Costa Rica Rift (Grim 1970) and from the Pacific–Antarctic Ridge (Herron 1972) exhibit no rotation pole shifts during this time. The complex pattern of anomalies over the Chile Ridge makes the estimated spreading direction uncertain (Klitgord *et al.* 1973), but the bathymetric relief indicates it was constant for the past 10 My. A transition to a new spreading direction is estimated to take several million years (Menard & Atwater 1968; Vogt *et al.* 1969), but velocities change abruptly in all of the cases we have examined, always in much less than a million years (Fig. 19). This, and the continuous pattern of identifiable anomalies, rule out the possibility that the observed accelerations are actually an artefact of changing spreading directions.

The Pacific–Antarctic Ridge has the longest interval between shifts (Fig. 19(a)). Vine (1966) compared anomaly spacings of the Eltanin-19 profile across the Pacific–Antarctic Ridge with those from a profile across the Juan de Fuca Ridge and concluded that there was a rate change at about 5 MyBP. There is still some uncertainty as to where this variation occurred, but comparison of the ages of the reversals in anomaly 3′ with palaeomagnetic data indicates that Vine was probably right in assuming that motion of the Pacific–Antarctic Ridge remained constant. Based on the Eltanin-19 profile, the eastern flank of the Pacific–Antarctic Ridge (Fig. 19(a)) seems to spread very erratically, but its velocity is the same as that of the western flank for long periods. This apparent instability could be caused by navigational errors, but it is also seen in the near-bottom profile over the east flank and might instead be due to a small offset in the crust at about 51° S. The Chile Rise decelerated at about 5 MyBP with constant motion before and after this time. Its rate and direction also changed at about 10 MyBP as part of the shift in plate motions which caused the spreading on the Galapagos Rise to cease (Herron 1972).

The three ridge segments bounded by the Pacific plate and a smaller plate (Juan de Fuca, Gorda and Rivera plates) slowed at 2 to 4 MyBP. A decrease of about 10 per cent on the west flank of the Juan de Fuca Ridge at 3 MyBP (Fig. 19(c)) agrees with spreading rates for the near-bottom profile on the eastern flank. The magnetic anomaly contour map of the north-east Pacific (Raff & Mason 1961) shows that the change in spreading on the Gorda Rise (Fig. 19(c)) occurred on both flanks, but the fracturing of the Gorda plate makes it difficult to find a good magnetic profile across the east flank. Further south, a similar variation occurs on both flanks of the East Pacific Rise at 21·5° N.

Changes in the total spreading rate on ridges are caused by variations in the plate motions of one or both plates meeting at the ridge, probably resulting in a new pole of relative motion. Some of the scatter in the determinations of poles of rotation (e.g. Chase 1972) could be caused by these small, unrecognized breaks in distance-age curves. The Pacific and Antarctic plates have maintained the same relative pole of rotation for the last 6 My, but all other plates in the Pacific have altered their motions At about 5 MyBP the Nazca plate motion was reoriented, producing a decrease in the spreading rate at the south on the Chile Ridge, and the rate changes at the north on the Costa Rica Rift. Velocities should also have varied on the East Pacific Rise between the Galapagos triple junction and the triple junction at 35° S, but the anomalies along most of this boundary are not identifiable because of the proximity to the magnetic equator and the strike of the ridge (Herron 1972). If the Pacific plate has moved uniformly, at least with respect to the Antarctic plate, the decelerations on the Juan de Fuca Ridge, Gorda Rise, and East Pacific Rise were caused by slowing of the three small plates as they were being subducted along the margin of the North American plate. A decrease in spreading rate also has been proposed for the Mid-Atlantic Ridge at 4 MyBP (Phillips *et al.* 1969; Vogt *et al.* 1969), and the south-east Indian Ridge at 80° E appears to have slowed at 3 MyBP (Fig. 19(b)). This suggests a large reshaping of plate motions between 2 and 4 MyBP.

A further possible departure from the ideal sea-floor spreading model of uniform symmetric motion, is asymmetric spreading with different half-rates on each flank of a ridge. Several studies indicate that this type of motion may be a common phenomenon. Both the Indian–Antarctic Ridge (Weissel & Hayes 1971; Schouten & McCamy 1972) and the Mid-Atlantic Ridge at 45° N (Loncarevic & Parker 1971) are probably examples of continuous asymmetric crustal accretion. Fig. 19(d) shows that the two flanks of the Costa Rica Rift have moved with different uniform velocities for the past 4–5 My. If this asymmetry is due to ridge jumps, they must be very small because of the constant spreading rates and lack of replicated anomalies. The location of intrusions and associated extrusions of new crust probably shifts in the formation zone and may move steadily southward on the Costa Rica Rift with

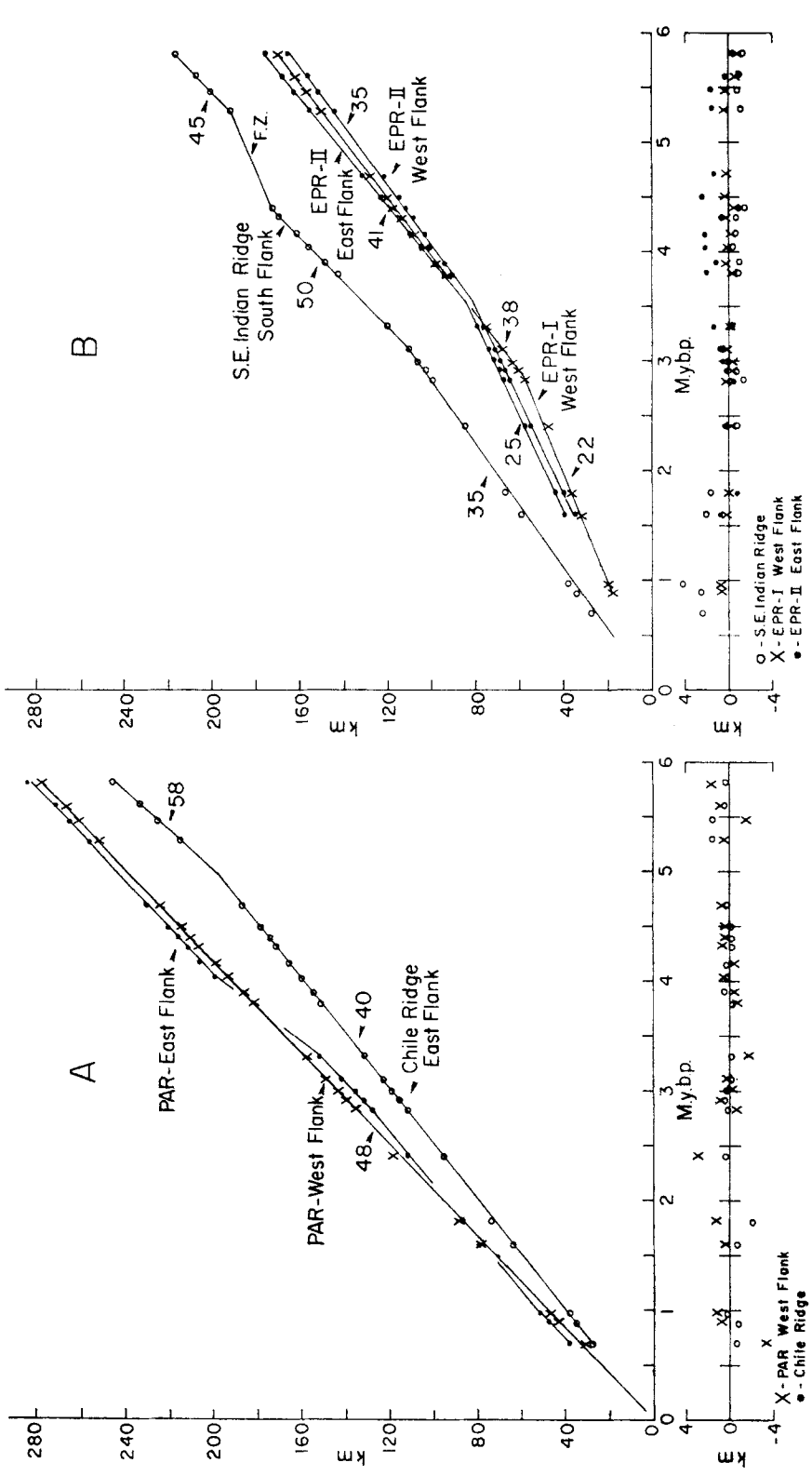

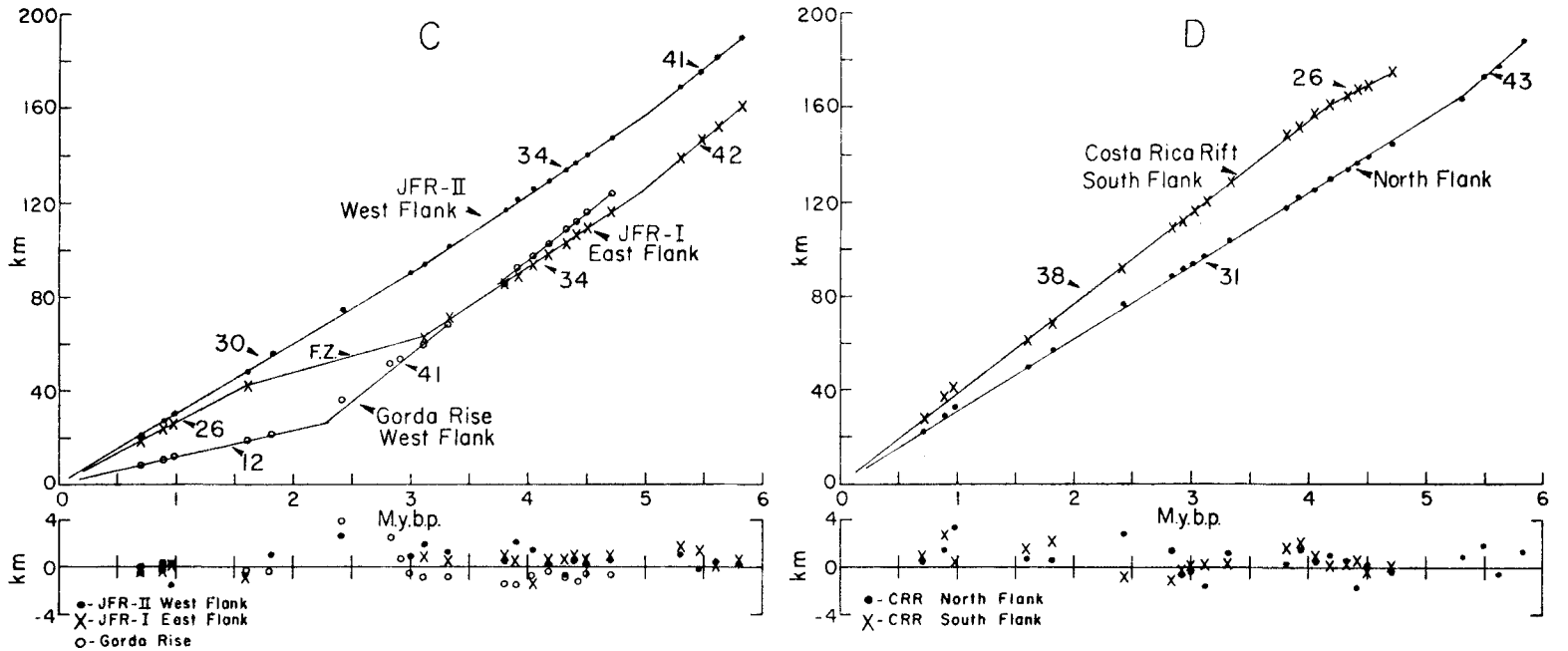

FIG. 19. Periods of constant spreading indicated by the straight line segments on the graphs of the distance to magnetic reversal boundaries *vs* the age of these boundaries using the time scale from Table 2. The spreading half-rates in mm/yr are indicated next to the various straight line segments. Portions of profiles which crossed fracture zones are indicated by FZ. Plotted below each of the graphs are the differences between the observed distances and those calculated using the spreading half-rates of Figs 16 and 18. The differences of distance have not been shown for the Eltanin-19 profile (PAR-East Flank) because of its apparent large spreading rate variations. The EPR-II West Flank differences have been omitted for reasons of clarity. A—Pacific–Antarctic Ridge (PAR): PAR-East Flank (El-19, Pitman & Heirtzler 1966); PAR-West Flank (Fig. 7); Chile Ridge: East Flank (SOUTHTOW-2, Klitgord *et al.* 1973). B—South-East Indian Ridge: South Flank (CONRAD 11·5, McKenzie & Sclater 1971); East Pacific Rise (EPR): EPR-I West Flank (Fig. 4); EPR-II West Flank and East Flank (GAM II, Fig. 17). C—Juan de Fuca Ridge (JFR): JFR-I East Flank (Fig. 2); JFR-II West Flank (composite, Vine 1966); Gorda Rise: West Flank (Fig. 3). D—Costa Rica Rift (CRR): CRR South Flank (Fig. 6); CRR North Flank (Profile E, Fig. 17).

respect to the Cocos plate. Our data cannot distinguish between small, discrete jumps and continuous migration. We can claim, however, that the jumps must be less than about 5 km in order to produce a spacing between reversal boundaries so close to that due to uniform spreading. There was a rate increase on the south flank

Table 2

The revised geomagnetic time scale determined from the 5 long deep tow profiles and the 2 surface ship profiles using the spreading rates given in Figure 16. This scale is the average of the ages determined from each of the ridges separately and the standard deviations of these ages are indicated. The time scales of Cox (1969) *and Talwani* et al. (1971) *are given for comparison. The ages of the edge of the central anomaly and the youngest and oldest boundaries of anomaly 2′ have been assumed known since there is a considerable amount of rock palaeomagnetic data around these three boundaries; the errors indicated by the standard deviations are not absolute but depend on these 3 ages being exact.*

	Geomagnetic time scale			
Anomaly	Cox (1969) (MyBP)	Talwani *et al.* (1971) (MyBP)	This paper (MyBP)	Standard deviation (My)
Central	0·00	0·00	0·00	—
	0·69	0·69	0·70*	0·03
Jaramillo	0·89	0·89	0·89	0·04
	0·95	0·95	0·95	0·05
2	1·63	1·71	1·62	0·03
	1·79	1·86	1·83	0·03
2′·1	2·43	2·43	2·41*	0·04
	2·80	2·84	2·84	0·04
2′·2	2·90	2·94	2·91	0·01
	2·94	3·04	3·00	0·01
2′·3	3·06	3·10	3·10	0·02
	3·32	3·32	3·32*	0·02
3·1	3·70	3·78	3·79	0·01
	3·92	3·88	3·89	0·01
3·2	4·05	4·01	4·02	0·01
	4·25	4·17	4·16	0·01
3·3		4·31	4·31	0·01
		4·41	4·38	0·01
3·4		4·48	4·48	0·01
		4·66	4·68	0·01
3′·1		5·18	5·25	0·03
		5·58	5·43	0·03
3′·2		5·66	5·58	0·01
		5·94	5·79	0·02

*Ages determined from rock palaeomagnetic data.

at about 4 MyBP, while the north flank slowed at 5·5 MyBP. If the low rate on the southern flank had persisted prior to 5·5 MyBP, the total accretion rate would be the same as that from 0 to 4 MyBP. These changes happen at different times on the two flanks, but this may be associated with the formation of the Carnegie Ridge at about this time (Anderson *et al.* 1975).

These calculations required dating the reversal boundaries from the absolute spreading velocities of each ridge, as described above. Surface profiles over the Chile Ridge at 40° S, 92° W (Klitgord *et al.* 1973) and the Southeast Indian Ridge at 41° S, 80° E (McKenzie & Sclater 1971) extended the magnetic coverage to segments of other fast spreading ridges not crossed with the deep-tow. Table 2 shows the resulting revised time scale for major polarity events during the last 6 MyBP. Our scale differs only slightly from that of Talwani *et al.* (1971), with the greatest differences at anomalies 2 and 3′. In the case of anomaly 2, our times are in closer agreement with those of Cox (1969). An agreement of this revised time scale with the published rock paleomagnetic data (Dalrymple 1972) is remarkably good, even for the ages between 5 and 6 MyBP. The similarity of this time scale to that of Talwani *et al.* (1971) indicates that the Reykjanes Ridge also has been spreading at a constant rate for the last 5 My (within the accuracies of choosing reversal boundaries on a slow spreading ridge).

8. Conclusions

We have found that magnetization solutions, constructed from near-bottom profiles over six ridge segments in the East Pacific, show alternate zones of positively and negatively magnetized material. These often closely approximate the ' box car ' structure predicted by sea floor spreading theory. We estimate the average transition zone width at reversal boundaries to be 2–3 km, independent of age or spreading half-rate. This smoothing places a lower limit of about 10 000 years on the duration of short events detectable with near-bottom data.

The magnetic anomaly from a uniformly magnetized layer model shows that the bathymetric relief produces significant short-wavelength (<3 km) components in the observed field. Our magnetization solutions, however, must also contain short-wavelength variations, which are particularly pronounced in the central anomaly. These are likely to be due to shortcomings in our simple constant-thickness model, rather than representing basalt heterogeneities or field strength fluctuations.

All six profiles show a gradual decrease in magnetization with age on the ridge flanks. The Gorda Rise, Galapagos Spreading Center and Pacific–Antarctic Ridge also exhibit a well-defined narrow zone of very high magnetization directly over the center of spreading. Rapid weathering of the fine-grained outer layer of pillow basalts could account for the narrowness of the central high; the more gradual decrease in magnitude on the flanks may be due to slower weathering of the larger-grained interiors. The nature of transition zones and magnetization amplitude over older crust may differ from that found here. The average magnetization may stabilize at a fairly low level at distances where the pillows are completely weathered leaving a signal only from deeper, more weakly magnetized material. This material cooled so slowly that apparent transition zone widths might be very wide, possibly accounting for the difference in widths found by Atwater and Mudie (1973) in very young crust, and Blakely and Cox (1972b) on early Cenozoic crust. The existence of a central magnetization high and a gradual amplitude decay on the flanks can probably be investigated with surface measurements, but these other conjectures are perhaps better tested with deep-tow data.

Reversal boundary locations from the profiles, coupled with palaeomagnetic data, provide a history of spreading variations in the Pacific and of the major polarity

events of the Earth's magnetic field. Short events are suggested on some profiles but our data will not clearly resolve them. Near-bottom and surface data show that spreading in the Pacific is not a uniform process. We find that a ridge's spreading history typically comprises long periods of constant motion, averaging several million years, separated by sudden changes in velocity. In particular, most of our ridges changed their motion at about 5 MyBP and at about 2–3 MyBP. Our revised geomagnetic time scale from 0–6 MyBP is in excellent agreement with rock paleomagnetic data and gives constant spreading from 0–5 MyBP on the Pacific–Antarctic Ridge, the Chile Ridge, the Costa Rica Rift and the Reykjanes Ridge. The extension of the time scale from 5–6 MyBP is based upon continued constant spreading on the Pacific–Antarctic Ridge and constant spreading on the East Pacific Rise (21° N) from 3–6 MyBP.

Although these results were obtained primarily for ridges in the east Pacific, there is no reason to suspect that these phenomena are confined to this region. The widespread occurrence of frequent velocity jumps in the last 6 million years leads us to propose that they reflect the constant readjustments required to follow the kinematically necessary shift in the poles of motion. We predict that such accelerations will be found wherever sufficiently detailed studies of the plate velocities can be made.

Acknowledgments

We are grateful to T. Atwater, J. Hawkins, P. Lonsdale and F. N. Spiess for their discussions, comments and criticisms. The deep-tow data were collected over a number of years and these cruises involved most of the students and engineering staff belonging to the deep-tow group led by F. N. Spiess. We thank them and the officers and crews of the RV *Oconostoto*, RV *Thomas Washington* and the USNS *De Steiguer*.

The Surveyor seismic profile was kindly provided by J. B. Grant at the NGSDC, NOAA.

This work was supported by the Office of Naval Research and grants NSF GA 31377X and NSF DES72–01650 from the National Science Foundation.

K. D. Klitgord and J. D. Mudie;
Marine Physical Laboratory of the Scripps Institution of Oceanography,
University of California at San Diego,
La Jolla, California 92037.

S. P. Huestis and R. L. Parker;
Institute of Geophysics and Planetary Physics,
University of California at San Diego,
La Jolla, California 92037.

References

Anderson, R. N., Clague, D. A., Klitgord, K. D., Marshall, M. & Nishimori, R. K., 1975. Magnetic and petrologic variations along the Galapagos Spreading Center, and their relation to the Galapagos melting anomaly, *Bull. geol, Soc. Am.*, **86**, 683–694

Atwater, T., 1970. Implication of plate tectonics for the Cenozoic tectonic evolution of western North America, *Bull. geol. Soc. Am.*, **81**, 3513–3536.

Atwater, T. M. & Mudie, J. D., 1968. Block faulting on the Gorda Rise, *Science*, **159**, 729–731.

Atwater, T. M. & Mudie, J. D., 1973. Detailed near-bottom geophysical survey of the Gorda Rise, *J. geophys. Res.*, **78,** 8665–8686.

Blakely, R. J., 1974. Geomagnetic reversals and crustal spreading rates during the Miocene, *J. geophys. Res.*, **79.** 2979–2985.

Blakely, R. J. & Cox, A., 1972a. Identification of short polarity events by transforming marine magnetic profiles to the pole, *J. geophys. Res.*, **77,** 4339–4349.

Blakely, R. J. & Cox, A., 1972b. Evidence for short geomagnetic polarity intervals in the Early Cenozoic, *J. geophys. Res.*, **77,** 7065–7072.

Blakely, R. J. & Schouten, H., 1974. Comments on ' Filtering marine magnetic anomalies ' by Hans Schouten and Keith McCamy, *J. geophys. Res.*, **79,** 773–774.

Bonhommet, N. & Babkine, J., 1967. Sur la presence d'aimantations iversees dans la Chaine des Puys, *C. R. Acad. Sci. Paris, Series B,* **264,** 92–94.

Bott, M. P. H. & Hutton, M. A., 1970. Limitations on the resolution possible in the direct interpretation of marine magnetic anomalies, *Earth. Planet. Sci. Lett.*, **8,** 317–319.

Brock, A. & Isaac, G. L., 1974. Paleomagnetic stratigraphy and chronology of hominid-bearing sediments east of Lake Rudolf, Kenya, *Nature,* **247,** 344–348.

Cande, S. C. & Labreque, J. L., 1974. Behaviour of the Earth's paleomagnetic field from small scale marine magnetic anomalies, *Nature,* **247,** 26–28.

Chase, C. G., 1972. The N-Plate Problem of plate tectonics, *Geophys. J. R. astr. Soc.*, **29,** 117–122.

Cox, A., 1969. Geomagnetic reversals, *Science,* **163,** 237–245.

Dalrymple, G. B., 1972. Potassium-argon dating of geomagnetic reversals and North American glaciations, *Calibration of Hominid Evolution,* 107–134. eds W. W. Bishop and J, A. Miller, Scottish Academic Press, Edinburgh.

Elvers, D., Srivastava, S. P., Potter, K., Morley, J. & Sdidel, D., 1973. Asymmetric spreading across the Juan de Fuca and Gorda Rises as obtained from a detailed magnetic survey, *Earth. Planet. Sci. Lett.*, **20,** 211–219.

Emilia, D. A. & Heinrichs, D. F., 1971. Ocean-floor spreading: Minor events in the Brunhes and the Matuyama epochs, (Abstract) EOS, *Trans. Am. geophys, Un.*, **52,** 824.

Gass, I. G. & Masson-Smith, D., 1963. The geology and gravity anomalies of the Troodos Massif, Cyprus, *Phil. Trans. R. Soc., Lond. A.*, **255,** 417–467.

Grim, P. J., 1970. Connection of the Panama Fracture Zone with the Galapagos Rift Zone, eastern tropical Pacific, *Mar. geophys. Res.*, **1,** 85–90.

Gromme, C. S. & Hay, R. L., 1967. Geomagnetic polarity epochs: New data from Olduvai Gorge, Tanganyika, *Earth. Planet. Sci. Lett.*, **2,** 111–115.

Heirtzler, J. R., Dickson, G. O., Herron, E. M., Pitman, III, W. G. & Le Pichon, X., 1968. Marine magnetic anomalies, geomagnetic field reversals and motions of the ocean floor and continents, *J. geophys. Res.*, **73.** 2119–2136.

Herron, E. M., 1972. Sea-floor spreading and the Cenozoic history of the east-central Pacific, *Bull. geol. Soc. Am.*, **83,** 1671–1692.

Hey, R. N., Johnson, G. L. & Lowrie, A., 1973. Recent apparent asymmetrical spreading near the Galapagos hot spot, *EOS, Trans. Am. geophys. Un.*, **54,** 244.

IAGA Commission Two Working Group 4, 1969. Analysis of the geomagnetic field, International Geomagnetic Reference Field, 1965, *J. geophys. Res.*, **74,** 4407–4408.

IDOE, 1971. Surveyor SEAMAP, NOAA Environmental Data Service, Washington D.C.

Irving, E., Robertson, W. A. & Aumento, F., 1970. The Mid-Atlantic Ridge near 45° N, VI. Remanent intensity, susceptibility, and iron content of dredge samples, *Can. J. earth Sci.*, **7,** 226–238.

Ivers, W. D. & Mudie J., D., 1973. Towing a long cable at slow speeds: A three-dimensional dynamic model, *Mar. Tech. Soc. J.*, **7,** 23–31.

Kay, R. N., Hubbard, N. J. & Gast, P. W., 1970. Chemical characteristics and origin of oceanic ridge volcanic rocks, *J. geophys. Res.*, **75,** 1585–1613.

Kendall, M. G. & Stuart, A., 1967. *The Advanced Theory of Statistics, Vol. 2–Inference and Relationship*, 2nd Edition, Hafner Publishing Co., New York.

Klitgord, K. D., 1975. Sea-floor spreading: The central anomaly magnetization high, *Earth Planet. Sci. Lett.*, submitted.

Klitgord, K. D. & Mudie, J. D., 1974. The Galapagos Spreading Centre: A near-bottom geophysical survey, *Geophys. J. R. astr. Soc.*, **38,** 563–586.

Klitgord, K. D., Mudie, J. D., Larson, P. A. & Grow, J. A., 1973. Fast sea-floor spreading on the Chile Ridge, *Earth Planet. Sci. Lett.*, **20,** 93–99.

Klitgord, K. D., Mudie, J. D. & Normark, W. R., 1972. Magnetic lineations observed near the ocean floor and possible implications on the geomagnetic chronology of the Gilbert epoch, *Geophys. J. R. astr. Soc.*, **28,** 35–48.

Larson, R. L., 1970. Near-bottom studies of the East Pacific Rise crest and tectonics of the mouth of the Gulf of California, Scripps Inst. Oceanogr. Ref. 70–72, La Jolla, Calif., 166 pp.

Larson, R. L., 1971. Near-bottom geophysical studies of the East Pacific Rise crest, *Bull. geol. Soc. Am.*, **82,** 823–842.

Larson, R. L., 1972. Bathymetry, magnetic anomalies, and plate tectonic history of the mouth of the Gulf of California, *Bull. geol. Soc. Am.*, **83,** 3345–3360.

Larson, R. L., Menard, H. W. & Smith, S. M., 1968. The Gulf of California: A result of ocean-floor spreading and transform faulting, *Science*, **161,** 781–784.

Le Pichon, X., 1968. Sea floor spreading and continental drift, *J. geophys. Res.*, **73,** 3661–3697.

Loncarevic, B. D. & Parker, R. L., 1971. The Mid-Atlantic Ridge near 45° N. XVII. Magnetic anomalies and ocean floor spreading, *Can. J. earth. Sci.*, **8,** 883–898.

Marshall, M. & Cox, A., 1971. Magnetism of pillow basalts and their petrology, *Bull. geol. Soc. Am.*, **82,** 537–552.

Marshall, M. & Cox, A., 1972. Magnetic changes in pillow basalts due to sea-floor weathering, *J. geophys. Res.*, **77,** 6459–6469.

McDougall, I. & Aziz-Ur-Rahman, 1972. Age of the Gauss-Matuyama boundary and of the Kaena and Mammoth events, *Earth Planet. Sci. Lett.*, **14,** 367–380.

McDougall, I. & Watkins, N. D., 1973. Age and duration of the Reunion geomagnetic polarity event, *Earth Planet. Sci. Lett.*, **19,** 443–452.

McDougall, I. & Wensink, H., 1966. Paleomagnetism and geochronology of the Pliocene–Pleistocene lavas in Iceland, *Earth Planet. Sci. Lett.*, **1,** 232–236.

McKenzie, D. P. & Parker, R. L., 1974. Plate tectonics in w-space, *Earth Planet. Sci. Lett.*, **22,** 285–293.

McKenzie, D. P. & Sclater, J. G., 1971. The evolution of the Indian Ocean since the Late Cretaceous, *Geophys. J. R. astr. Soc.*, **25,** 437–528.

Menard, H. W. & Atwater, T., 1968. Changes in direction of sea-floor spreading, *Nature*, **219,** 463–467.

Menard, H. W. & Mammerickx, J., 1967. Abyssal hills, magnetic anomalies and the East Pacific Rise, *Earth Planet. Sci. Lett.*, **2,** 465–472.

Miller, S. P., Klitgord, K. D. & Mudie, J. D., 1974. Influence of geological and time varying sources on the spectra of marine magnetic anomalies, (Abstract) *EOS Trans. Am. geophys. Un.*, **55,** 231.

Molnar, P. & Sykes, L. R., 1969. Tectonics of the Caribbean and Middle America regions from focal mechanisms and seismicity, *Bull. geol. Soc. Am.*, **80,** 1639–1684.

Moores, E. M. & Vine, F. J., 1971. The Troodos Massif, Cyprus and other ophiolites as oceanic crust: evaluation and implications, *Phil. Trans. R. Soc. Lond. A.*, **268,** 443–466.

Morgan, W. J., Vogt, P. R. & Falls, C. F., 1969. Magnetic anomalies and sea-floor spreading on the Chile Rise, *Nature*, **222,** 137–142.

Mudie, J. D., Grow, J., Klitgord, K. D. & Larson, P., 1972. *Shipboard cruise report on Leg 2 of Expedition SOUTHTOW: Studies in the southeast Pacific*, Scripps Inst. Oceanography Ref. 72–66, La Jolla, Calif., 40 pp.

Opdyke, N. D. & Foster, J., 1970. The paleomagnetism of cores from the North Pacific, *Geol. Soc. Am. Mem.*, **126,** 83–120.

Parker, R. L., 1973. The rapid calculation of potential anomalies, *Geophys. J. R. astr. Soc.*, **31,** 447–455.

Parker, R. L. & Huestis, S. P., 1974. The inversion of magnetic anomalies in the presence of topography, *J. geophys. Res.*, **79,** 1587–1593.

Parker, R. L. & Klitgord, K. D., 1972. Magnetic upward continuation from an uneven track, *Geophys.*, **37,** 662–668.

Peter, G. & Lattimore, R., 1969. Magnetic structure of the Juan de Fuca–Gorda Ridge area, *J. geophys. Res.*, **73,** 586–593.

Phillips, J. D., Thompson, G., Von Herzen, R. P. & Bowen, V. T., 1969. Mid-Atlantic Ridge near 43° N latitude, *J. geophys. Res.*, **74,** 3069–3081.

Pitman, W. C. & Heirtzler, J. R., 1966. Magnetic anomalies over the Pacific–Antarctic Ridge, *Science*, **154,** 1164–1171.

Raff, A. D. & Mason, R. G., 1961. A magnetic survey off the west coast of North America, 40° N to 52° N, *Bull. geol. Soc. Am.*, **72,** 1267–1270.

Schouten, H. & McCamy, K., 1972. Filtering marine magnetic anomalies, *J. geophys. Res.*, **77,** 7089–7099.

Schouten, J. A., 1971. A fundamental analysis of magnetic anomalies over oceanic ridges, *Mar. geophys. Res.*, **1,** 111–144.

Sclater, J. G., Anderson, R. N. & Bell, M. L., 1971. The elevation of ridges and the evolution of the Central Eastern Pacific, *J. geophys. Res.*, **71,** 7888–7915.

Sclater, J. G. & Klitgord, K. D., 1973. A detailed heat flow, topographic and magnetic survey across the Galapagos Spreading Centre at 86° W., *J. geophys. Res.*, **78,** 6951–6975.

Shor, G. G., Dehlinger, P., Kirk, H. K. & French, W. S., 1968. Seismic refraction studies off Oregon and Northern California, *J. geophys. Res.*, **73,** 2175–2193.

Silver, E. A., 1969. Late Cenozoic underthrusting of the continental margin off northernmost California, *Science*, **166,** 1265–1266.

Smith, J. D. & Foster, J. H., 1968. Geomagnetic reversal in Brunhes normal polarity epoch, *Science*, **163,** 565–567.

Spiess, F. N., Loughridge, M. S., McGehee, M. S. & Boegeman, D. E., 1966. An acoustic transponder system, *Navigation*, **13,** 154–161.

Spiess, F. N. Mudie, J. D., 1970. Fine-scale topographic and magnetic features of the sea floor, *The Sea*, **Vol. 4,** Part I, 205–250, ed. A. E. Maxwell, John Wiley & Sons, New York.

Spiess, F. N. & Sanders, S. M., 1971. *Survey of Chase Disposal Area (NITNATOW)*, Scripps Inst. Oceanogr. Ref. 71–33, La Jolla, Calif. 20 pp.

Spiess, F. N. & Tyce, R. C., 1973. *Marine Physical Laboratory deep tow instrumentation system*, Scripps Inst. Oceanogr. Ref. 73–4, La Jolla, Calif. 37 pp.

Talwani, M., Windisch, C. C. & Langseth, M. G., 1971. Reykjanes Ridge Crest: A detailed geophysical study, *J. geophys. Res.*, **76,** 473–517.

Vacquier, V., 1972. *Geomagnetism in marine geology*, 163–168. Elsevier, Amsterdam.

Vine, F. J., 1966. Spreading of the ocean floor: New evidence, *Science*, **154,** 1405–1415.

Vogt, P. R., Avery, O. E., Schneider, E. D., Anderson, C. N. & Bracey, D. R., 1969. Discontinuities in sea-floor spreading, *Tectonophys.*, **8,** 285–317.

Watkins, N. D., 1968. Short period geomagnetic polarity events in deep sea sediment cores, *Earth Planet. Sci. Lett.*, **4,** 341–349.

Watkins, N. D. & Abdel-Monem, A., 1971. Detection of the Gilsa Geomagnetic polarity events on the island of Madeira, *Bull. geol. Soc. Am.*, **82,** 191–198.

Watkins, N. D., Paster, T. & Ade-Hall, J., 1970. Variations of magnetic properties in a single deep-sea pillow basalt, *Earth Planet. Sci. Lett.*, **8**, 322–328.

Weissel, J. K. & Hayes, D. E., 1971. Asymmetric sea-floor spreading south of Australia, *Nature*, **231**, 518–522.